Modeling and Control of the Hybrid Power Flow Controller for Steady-state and Dynamic Studies and Applications

by

Behnam Tamimi

A thesis
presented to the University of Waterloo
in fulfillment of the
thesis requirement for the degree of
Doctor of Philosophy
in
Electrical and Computer Engineering

Waterloo, Ontario, Canada, 2017

Examining Committee Membership

The following served on the Examining Committee for this thesis. The decision of the Examining Committee is by majority vote.

External Examiner:	Rajiv K. Varma Professor, Dept. of ECE, University of Western Ontario
Supervisor:	Claudio A. Cañizares Professor, Dept. of ECE, University of Waterloo
Internal Member:	Kankar Bhattacharya Professor, Dept. of ECE, University of Waterloo
Internal Member:	Mehrdad Kazerani Professor, Dept. of ECE, University of Waterloo
Internal-External Member:	Kumaraswamy Ponnambalam Professor, Dept. of SDE, University of Waterloo

I hereby declare that I am the sole author of this thesis. This is a true copy of the thesis, including any required final revisions, as accepted by my examiners.

I understand that my thesis may be made electronically available to the public.

Abstract

Flexible ac transmission system (FACTS) controllers offer new opportunities to better control power systems, and can address some of the critical challenges faced by the grid, especially in the context of smart grids. Furthermore, the smartening of distribution systems with distributed generation, storage devices, and intelligent loads have created challenges for the operation of distribution feeders, which can be addressed adequately with power-electronics based controllers and FACTS controllers for distribution systems. However, the capital intensive nature of these controllers is a major obstacle for a wide application of this technology in power systems. A cost effective FACTS controller has been introduced in the literature, which yields operating characteristics similar to those of the versatile Unified Power Flow Controller (UPFC). This device consists of converters as well as passive components, and is referred to as the Hybrid Power Flow Controller (HPFC). The study of the HPFC and its performance in electric power systems requires adequate and relevant models representing the device behavior according to the intended studies, such as steady state or time-domain dynamic analyses; moreover, the benefits of an HPFC are determined by its limits and operating constraints. Therefore, static and dynamic models of the HPFC for transmission and distribution system applications are proposed and studied in this work.

First, steady-state models of the HPFC for power flow and optimal power flow (OPF) studies are proposed in this work, considering its multiple control modes and operating constraints. Thus, a strategy for control limit handling in power flow calculations is proposed, while considering a discrete passive shunt capacitor bank in the device. Moreover, an OPF model of the device is proposed and explained in detail, representing all the device control and physical limits as constraints in the mathematical formulation, so that the HPFC can be optimally dispatched as a part of the transmission system control assets; this model is used to determine the optimal ratings of the device based on a cost–benefit analysis. The proposed power flow and OPF models are tested and validated based on several loadability studies on a two-area benchmark test system. The HPFC power flow model is also tested and applied to a detailed model of Ontario grid and its neighboring networks with more than 6000 buses. The analyses demonstrate the application of the models for planning and operation studies, evaluating the performance and the effectiveness of the device based on realistic studies and scenarios.

Second, the merits and the added value of the HPFC application to distribution systems are discussed here through detailed modeling and time-domain simulations, examining its impact on a distribution network under different conditions. Thus, a detailed dynamic representation of the HPFC is developed and implemented in PSCAD/EMTDC, describing

and proposing control strategies to properly operate this controller in distribution system applications, such as an effective and simple procedure for starting-up the device. The developed model is used to demonstrate the effectiveness of the controller for solving problems in distribution systems, such as voltage sags associated with feeder faults and power flow fluctuations due to intermittent renewable generation using a benchmark network as an illustrative example.

Acknowledgements

I would like to express my sincere gratitude to my supervisor Professor Claudio A. Cañizares for his invaluable trust, support, guidance, and patience during the course of my studies at the University of Waterloo. His professionalism, thoughtful guidance, and encouragement have helped me walk through various stages of my work during the years of my research and study at Waterloo. Moreover, his passion and extraordinary dedication to teaching and research have always inspired me, and encouraged me to work harder and better.

My appreciation extends to my Ph.D. Committee members for their valuable comments and inputs. They are: Professor Kankar Bhattacharya from the Electrical and Computer Engineering Department at the University of Waterloo; Professor Mehrdad Kazerani from the Electrical and Computer Engineering Department at the University of Waterloo; Professor Kumaraswamy Ponnambalam from the Systems Design Engineering Department at the University of Waterloo; and Professor Rajiv K. Varma from the Electrical and Computer Engineering Department at the University of Western Ontario.

My warmest thanks and endless appreciations to my family and especially my mother for their years of unconditional support, encouragement, and true love even when I could not truly appreciate their sacrifices. Nothing would have been possible without their devotion.

I warmly thank my friends and colleagues in the Electricity Market Simulation and Optimization Lab (EMSOL) who have given me a great deal of support and provided a pleasant work environment in the years of my studies. I am tempted to individually thank each of them, but as the list is long and to not unintentionally omit someone, I am not including their names here. However, I would like to especially thank my dear friend Dr. Ehsan Nasr Azadani for his constant presence and kind words.

I wish to express my warm and sincere thanks to Professor Sadegh Vaez-Zadeh, my supervisor during my studies at the University of Tehran, Tehran, Iran, whose kindness and encouragement have always been a true source of inspiration for me during all these years before and after I left my home country. I would also like to thank the kind and helpful staff at the Electrical and Computer Engineering Department at the University of Waterloo, including Ms. Susan Widdifield and Ms. Brenda McQuarrie for their support, patience, and understanding.

Finally, I gratefully acknowledge the funding and support provided by the Natural Sciences and Engineering Research Council (NSERC) of Canada, Ontario Centres of Excellence (OCE), Hydro One Networks Inc., and Mathematics of Information Technology and Complex Systems (MITACS) to carry out my research.

Dedication

This is dedicated to my mother.

Table of Contents

List of Tables

List of Figures

List of Acronyms

EMTDC	Electromagnetic Transients including DC
EMTP	Electromagnetic Transients Program
FACTS	Flexible ac Transmission Systems
GS	Gauss-Seidel
HPFC	Hybrid Power Flow Controller
HVDC	High Voltage dc
IESO	Independent Electricity System Operator
LP	Linear Programming
NLP	Nonlinear Programming
NR	Newton-Raphson
OPF	Optimal Power Flow
PES	Power & Energy
PID	Proportional Integral Derivative
PI	Proportional Integral
PSAT	Power System Analysis Toolbox
PWM	Pulse Width Modulating
SPVG	Solar Photovoltaic Generator
SQP	Sequential Quadratic Programming
SSSC	Series Static Synchronous Compensator
STATCOM	Static Synchronous Compensator
SVC	Static VAR Compensator
UPFC	Unified Power Flow Controller
VSC	Voltage Source Converter

List of Symbols

B_{kl}	Imaginary part of $\boldsymbol{y}_{kl}$
$C_k(\cdot)$	Production cost of generator k
C	Capacitor value at the converter output
$F(\cdot)$	Equality constraints in OPF formulation
$\mathcal{G}$	Set of generators
G_{kl}	Real part of $\boldsymbol{y}_{kl}$
G	Sensitivity matrix in PQQ mode calculations
$H(\cdot)$	Transmission system limits in OPF formulation
$\boldsymbol{I}_k$	Current phasor injected into bus k
K	Multiplying factor in PQQ mode calculations
L	Inductor value at the converter output
$\mathcal{N}$	Set of all buses
P_1	Active power flowing into HPFC Terminal 1
P_2	Active power flowing out of HPFC Terminal 2
P_{Dk}	Active power of load k
P_{Gk}	Active power of generator k
P_k	Injected active power at bus k
Q_1	Reactive power flowing into HPFC Terminal 1
Q_2	Reactive power flowing out of HPFC Terminal 2
Q_{Dk}	Reactive power of load k
Q_{Gk}	Reactive power of generator k
Q_k	Injected reactive power at bus k
R	Represents converter losses
$\boldsymbol{V}_k$	Voltage phasor at bus k
B_M	Shunt device susceptance value
$_d$	Subscript for instantaneous d-component vlaue in dq-reference frame

δ_k	Phase angle at bus k
$\Delta P_{dc}/2$	Auxiliary signal for loss compensations
f_s	Switching frequency (Hz)
I_{dc}	Average dc-capacitor current
i, m, n	Dummy variables
$\boldsymbol{I}_R$	Current phasor flowing out of HPFC Terminal 2
$\boldsymbol{I}_S$	Current phasor flowing into HPFC Terminal 1
i_{ta}	Instantaneous filtered value of converter output current for Phase a
K_i	Integrating factor of PI controller
k, l	Bus numbers
K_p	Gain of PI controller
$_q$	Subscript for instantaneous q-component vlaue in dq-reference frame
τ	Control loop time constant
$\boldsymbol{V}_1$	HPFC Terminal 1 voltage phasor
$\boldsymbol{V}_2$	HPFC Terminal 2 voltage phasor
ε	Small tolerance in calculations
V_{dc}	DC-capacitor voltage
v_{ga}	Instantaneous voltage generated by the switches for Phase a
$\boldsymbol{V}_M$	Shunt device voltage phasor
v_{ta}	Instantaneous filtered value of v_{ga}
$\boldsymbol{V}_X$	Series voltage phasor representing HPFC Converter 1
$\boldsymbol{V}_Y$	Series voltage phasor representing HPFC Converter 2
w_s	Switching frequency (rad/s)
$\boldsymbol{y}_{kl}$	(k, l) entry in the bus admittance matrix

Chapter 1

Introduction

1.1 Motivation

The bulk of electric power delivered to electricity costumers is transferred through high-voltage transmission lines and medium/low-voltage distribution networks, with each part facing various challenges and issues in light of new regulations, requirements, and technical developments in the context of competitive electricity markets and smart grids. In transmission systems, high penetration levels of centralized renewable energy sources, strict regulations and ever-changing demand patterns, as well as competition among electricity market participants have created new and hard-to-predict flow patterns. Existing aging transmission networks have not been designed to accommodate these power flows, which many times push the grid to its capability limits; thus, an effective solution to address this challenge has been devised based on power electronic components, referred to as Flexible ac Transmission Systems (FACTS) [1]. On the other hand, at lower voltage levels in power distribution networks, the smartening of the system with distributed generation, storage devices, and intelligent loads have created challenges for the operation of distribution feeders, which can be addressed with power-electronics based controllers tailored for distribution systems [2], [3]. Thus, several FACTS controllers have been proposed in the literature, including Static Synchronous Compensators (STATCOMs), Series Static Synchronous Compensators (SSSCs), and Unified Power Flow Controllers (UPFCs) and their distribution-oriented counterparts [4]–[6]. Among these controllers, the UPFC is probably the most versatile, as it can control various system variables independently, particularly bus voltage magnitudes and transmission line active and reactive power flows [7], [8].

Although FACTS controllers have proved to be capable of controlling voltages and

flows adequately, their capital-intensive nature has impeded their wide utilization in power systems. For instance, as of today, only a few large and functional UPFC installations with ratings greater than 10 MVA are reported in the literature. Thus, a cost effective FACTS controller is introduced and presented in [9], which yields operating characteristics similar to those of the UPFC while requiring a lower capital investment. This device consists of converters as well as passive components (e.g. capacitor banks), and is referred to as the Hybrid Power Flow Controller (HPFC). Compared to the UPFC, the savings stem from a few structural differences between the two controllers, including the use of half-sized converters and passive elements for supplying the bulk of the required reactive power.

The study of the HPFC and its performance in power systems at any voltage level requires adequate and relevant models representing the device behavior based on the intended studies, such as steady state or time-domain dynamic analyses. Moreover, the benefits of an HPFC are determined by its limits and operating constraints; therefore, the impact of the device limits on its performance must be properly considered in the associated models. However, previously published works on the HPFC do not comprehensively discuss the device's modeling and its operating limits [9]–[12].

Given the interest by Hydro One [13] in studying the impact and benefits of introducing an HPFC in the Ontario grid, this research work considers and proposes power flow, optimal power flow (OPF), and detailed dynamic models of the HPFC. The power flow model represents the device and its operating limits for power flow analysis, which is one of the most widely used and important tools for power system studies. The OPF model can be used in operation and planning studies to optimize the intended variables, while respecting the capability limits of the HPFC and other components of the system. Finally, an HPFC model appropriate for time-domain studies allows evaluating the overall dynamic response of the system. Therefore, this research work provides essential tools and models to comprehensively study the impact and benefits of integrating an HPFC into practical power systems at different voltage levels.

1.2 Research Workflow

An outline of the research work presented here is depicted in Figure 1.1. It starts with reviewing previously published literature on the subject, including several relevant works on the modeling of the UPFC. Next, the basics of the HPFC and its structure are studied through preliminary modeling and simulations. The various developed models are constantly improved based on preliminary results and ongoing review of similar published works. After several debugging iterations to correct shortcomings in the models, these can

be implemented in different software packages based on the intended application, using them to perform relevant and practical power system studies.

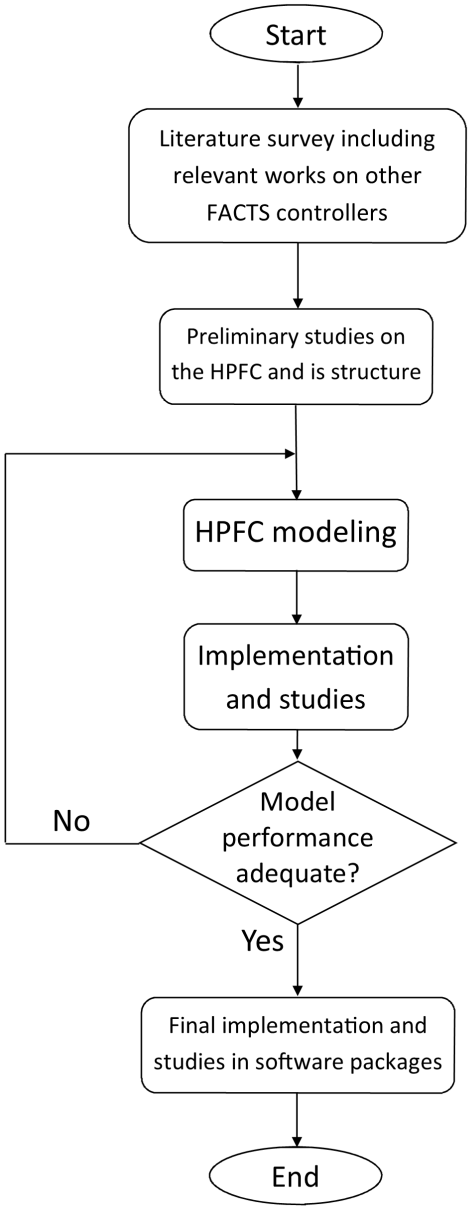

Figure 1.1: Work flow and different activities associated with the research work.

1.3 Literature Review

The HPFC with its main features and specifications were patented in the US in late 2005 under the title "Hybrid Power Flow Controller and method" [14]. In 2006, the main developers and patent owners presented and published the idea and the description of different components of the HPFC in a short paper in the IEEE Power & Energy (PES) General Meeting in Montreal, Canada [9]. Thus, since the HPFC was introduced relatively recently, there is a limited number of published works examining its modeling and operation [9]–[12]. These references are reviewed next, together with other relevant publications on the modeling of other related FACTS controllers, specifically the UPFC. Hence, one of the objectives of the present work, motivated by the interest of Hydro One in the technology, as previously mentioned, is to explore in detail the modeling and applications of the HPFC, to expose industry and other researchers to its merits and potential uses in power systems.

this lack of exposure to the industry and other researchers is another reason that motivated the current research work.

1.3.1 HPFC

The device is introduced in [14], and in [9] an interesting geometrical representation of the device's operating region is presented by the HPFC patent owners. An electromagnetic transients program (EMTP) model of the HPFC is briefly studied in [10], and the performance of the HPFC for improving the power transfer capability of a system is compared with that of the UPFC in [11], based on time domain simulations using PSCAD™/EMTDC™ [15]. The authors in [12] implemented and studied the HPFC as a stabilizer in Simulink® [16], by connecting two SSSCs and a Static VAR Compensator (SVC), without discussing in detail the control procedure and the device's capability limits. Therefore, the modeling of the HPFC and its operating limits for power system studies, which typically require power flow, OPF, and dynamic analyses, have not been studied adequately in the literature. Hence, given the interest on the application of this controller by Hydro One, this research work concentrates on developing appropriate models to comprehensively study the impact and benefits of the HPFC for the Ontario grid.

1.3.2 Similar FACTS Controller Models

Several valuable relevant works on UPFC modeling and associated limits have been reported in [7], [8], [17]–[23]. Static and dynamic models of the UPFC are presented in

[7] using modulation indices for power electronic switches. The controller equations are combined with the system power flow equations sequentially and iteratively; however, converters current limits are not considered in the reported simulations. In [17], the UPFC series and shunt inverters are represented by voltage and current sources, respectively, and a control scheme for the UPFC is proposed to maximize the active power flow through the line; the device operational constraints are managed by changing the series voltage phase angle accordingly. The authors assume that the voltage phasor at the shunt bus can be used as a reference for the controller, ignoring the voltage dynamics of the system, which may cause problems in a practical implementation. Steady-state power flow and voltage control studies are reported in [18], in which an iterative technique is used based on adjusting the controller set points and parameters, using a sequence of power flow solutions to handle controller limits in the power flow simulations; however, transients are ignored.

In [19], a FACTS controller is modelled as a fundamental frequency voltage source behind a reactance. The device is included in power flow calculations by adding relevant rows and columns to the system Jacobian. The limits on the device variables are checked after the power flow solution, and if violated, a new dispatch is calculated for the controller to remove the binding constraint. In other words, power flow solutions and sensitivity-based re-dispatch are iterated until there are no limit violations. The impact of converters' current and voltage constraints on the performance of the UPFC in improving a transmission line's loadability is examined in [8] ignoring the transients. The authors in [20] geometrically obtain a set of admissible solutions for a line with UPFC, assuming given parameters such as sending and receiving end voltages as well as the desired active power flow; this is a method that needs to be done offline and cannot be used to control the device.

In [21], a Newton-based power flow model is proposed for the UPFC considering its internal limits and using an augmented Jacobian for the system; however, it is assumed that the Jacobian matrix is accessible which is not always true. Finally, fundamental frequency models of UPFC and other FACTS controllers are presented in [22] and [23] for power flow and transient stability studies considering the converters limits and losses ignoring dynamic behavior at the switch level. Also, in [24], different popular topologies for converter-based FACTS are compared, and their benefits for integrating renewables in distribution systems are illustrated; however, it is shown that economy concerns can constrain the ratings of such controllers, resulting in limiting the possible applications of these controllers in distribution networks.

1.4 Research Objectives

The review of the current technical literature demonstrate the need for adequate HPFC models for steady state and time-domain dynamic studies. Thus, the objectives of the current research work are the following:

- Model the HPFC from the system point of view; thus, the device terminals should be considered in the power flow model, to be consistent with what a system operator requires from the device. The controllers internal variables should be properly represented to allow handling the device limits accurately, and thus modeling the multiple control modes of HPFC operation in steady state.
- Integrate the developed model into a standard power flow program using a sequential approach, thus allowing its integration into commercial power system analysis software packages, such as PSS®E [25]. This will allow to study the steady-state impact and benefits of the HPFC in a detailed and large model of the Ontario grid, based on voltage profiles and loadability studies.
- Develop a model of the HPFC for OPF applications, considering the device ratings and its control variables and limits directly. The proposed model will be used to demonstrate its application in planning and operation studies, evaluating the performance and the effectiveness of the device using in a test system, with practical assumptions and scenarios applicable to practical systems.
- Develop a model and controls of the HPFC for time-domain dynamic analyses and applications. This model will be used to study the dynamic performance of the HPFC in an electric power distribution system, utilizing an Electromagnetic Transient analysis package such as PSCAD/EMTDC, evaluating and demonstrating the controller's response to contingencies and fluctuations due to the presence of renewable energy resources in distribution networks.

1.5 Outline of the Thesis

The rest of the thesis is organized as follows:

- Chapter 2 provides a background review on the concepts and tools used in this research work, including various concepts associated with power flow and OPF modeling and solutions. A brief review of voltage-source converters, and the HPFC architecture, with its circuit model and associated operating modes, are also presented.

Relevant software packages which can be used to carry out the studies preformed in this research work are briefly discussed in this chapter as well.

- The proposed HPFC model for power flow applications is discussed in Chapter 3, elaborating on an effective strategy to handle the operating limits in steady state. Also, the results of integrating the HPFC in a two–area benchmark test system as well as a detailed Ontario grid model are presented and discussed, including several loadability studies to evaluate the performance and demonstrate the benefits of the HPFC in steady state.

- The proposed HPFC model for OPF applications is presented in Chapter 4, considering the operating limits of the controller and the network in steady state. The results of the application of the HPFC to a two–area benchmark test system are also presented and discussed, including several OPF studies to evaluate the performance and illustrate the benefits of optimally sizing and dispatching the HPFC.

- The proposed HPFC model for time-domain dynamic studies is discussed in Chapter 5, describing and proposing control strategies to properly operate this controller in distribution system applications, such as an effective and simple procedure for starting-up the device. The dynamic model of the controller is applied to a benchmark distribution system to evaluate its performance under fault conditions as well as flow fluctuations due to the presence of renewable energy resources.

- Chapter 6 summarizes the main conclusions and contributions of this thesis, and suggests possible future research work.

- The appendices present relevant information and data of the test system components and their corresponding controls used for simulations, including the two-area, Ontario, and CIGRE test systems.

Chapter 2

Background Review

This chapter presents a background review of the concepts, models, and tools that are used in this research work. First, the modeling approach and its required steps for the different applications considered in this work are discussed. Then, the basics of power flow and OPF formulation and solution methods relevant to the thesis are briefly presented. The fundamentals of Voltage Source Converters (VSCs) and their basic controls are reviewed next. Then, the general structure of the HPFC is discussed, highlighting its main features and components, and finally, popular software packages used in this work are presented.

2.1 Application-oriented Modeling

The details of the modeling and implementation phases of this work are illustrated in some detail in Figure 2.1. Modeling a component requires the knowledge of its behavior and relevant dynamics for the intended time frame. The phenomena of concern to the scope of this research work include dynamics relevant to electromagnetic transients as well as the steady-state performance in power system studies, for which appropriate models are developed. The intended application of the models determine the software packages and the associated implementation needed for the proposed studies. In other words, based on the intended application and required software package, the HPFC and its components are modeled using available building blocks and library components.

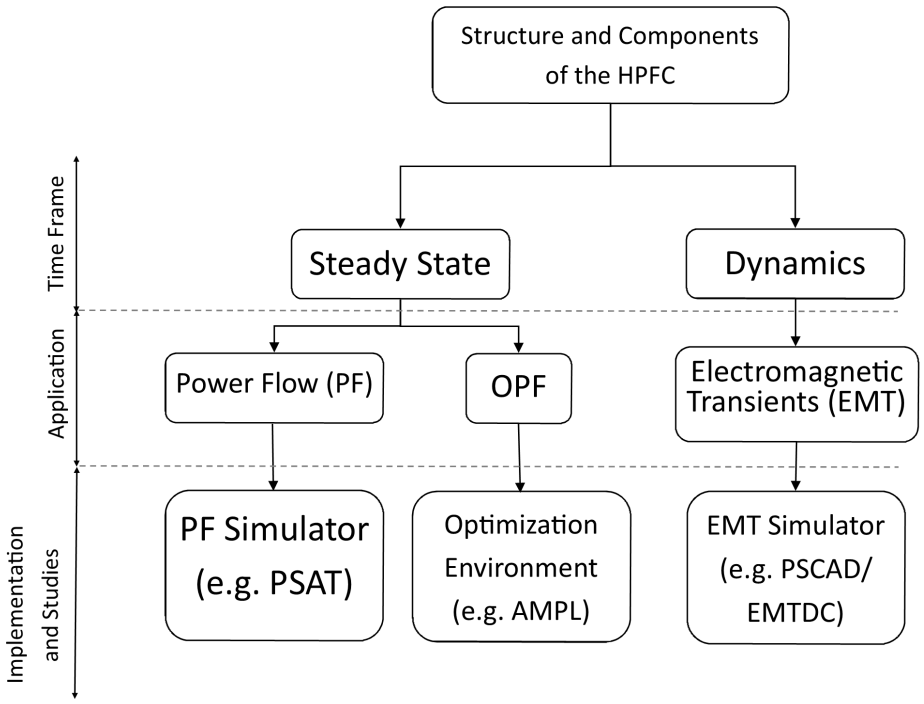

Figure 2.1: HPFC modeling and implementation overview.

2.2 Power Flow

Power flow calculations are used to determine the steady-state operating characteristics of a power system for a given set of loads and a pre-specified generation dispatch [26]. The solution provides information regarding voltage phasors, active and reactive power flows in branches, and power injections at different system nodes.

2.2.1 Problem Formulation

The phasor current injected into a bus k in a system is equal to [26]:

$$\boldsymbol{I}_k = \sum_{l \in \mathcal{N}} \boldsymbol{y}_{kl} \boldsymbol{V}_l \qquad \forall k \in \mathcal{N} \tag{2.1}$$

where $\mathcal{N}$ is the set of all buses, $\boldsymbol{V}_l$ is the voltage phasor at bus m, and $\boldsymbol{y}_{kl}$ represents the (k, l) entry in the bus admittance matrix. The complex power at a bus k is then given by:

$$\boldsymbol{S}_k = P_k + jQ_k = \boldsymbol{V}_k \boldsymbol{I}_k^* = V_k \angle \delta_k \sum_{l \in \mathcal{N}} \boldsymbol{y}_{kl}^* V_l \angle - \delta_k \qquad \forall k \in \mathcal{N} \tag{2.2}$$

where P, Q, V, and δ represent injected active power, injected reactive power, voltage magnitude, and voltage phase angle at a bus, respectively. The complex load flow equations are non-analytical, i.e. they cannot be differentiated in complex form [27]; therefore, the problem is usually written in the form of real equations and variables. Thus, assuming polar form, one has:

$$P_k = V_k \sum_{l \in \mathcal{N}} V_l (G_{kl} \cos \delta_{kl} + B_{kl} \sin \delta_{kl}) \qquad \forall k \in \mathcal{N} \tag{2.3}$$

$$Q_k = V_k \sum_{l \in \mathcal{N}} V_l (G_{kl} \sin \delta_{kl} - B_{kl} \cos \delta_{kl}) \qquad \forall k \in \mathcal{N} \tag{2.4}$$

where G_{kl} and B_{kl} are real and imaginary parts of $\boldsymbol{y}_{kl}$, and $\delta_{kl} = \delta_k - \delta_l$.

Equations (2.3) and (2.4) define the relationship between four main variables at each bus. Hence, the buses are classified based on the variables that are known at those nodes:

- Load bus (PQ): The active and reactive power demands are assumed to be known from load forecasts or measurements. Voltage magnitude and phase need then to be computed.
- The voltage controlled bus (PV): voltage magnitude is held constant at a pre-specified value, and the injected active power is also known; generator buses are good examples of these types of buses. In this case, Q and δ need to be computed. Voltage regulation capability may be lost when the bus capability limits are reached forcing the bus to become a PQ bus.
- Slack (swing) bus: The voltage magnitude and phase angle are known at this bus. P and Q are calculated at this bus.

This classification yields enough equations and known variables to be able to solve the associated set of nonlinear power flow equations defined by (2.3) and (2.4).

2.2.2 Solution Methods

There are different methods available for solving the nonlinear power flow equations iteratively, such as Gauss-Seidel (GS) and Newton-Raphson (NR) [26]. There is no "perfect" method and each one has its advantages/disadvantages; however, NR is the most popular one, because of its accuracy and low number of required iterations. The basics of this method are explained next.

The NR method iteratively improves the values of unknown variables through first-order approximations of the corresponding nonlinear functions. In other words, the nonlinear power flow equations are linearized for small variations in the variables V and δ and solved iteratively using a Jacobian matrix, which contains the derivatives of the nonlinear functions (2.3) and (2.4) representing P and Q as functions of V and δ. This iterative procedure is repeated until the error between the obtained values of (2.3) and (2.4) at two consecutive iterations becomes smaller than a threshold, at which point the algorithm stops and results are reported. One important drawback for the NR method is that its performance is strongly affected by the starting value of the variables; for instance, a flat start for a large system usually yields convergence problems. Hence, care must be taken to properly initialize the NR solution process.

2.2.3 FACTS Controller Integration

FACTS controllers, as versatile power flow controllers, are required to be adequately modeled and included in power flow calculations. There are two general approaches to incorporate power-electronics-based devices, such as High Voltage dc (HVDC) transmission lines, in these calculations, namely, unified and sequential solutions [27].

Unified Solution

The unified approach combines the equations pertaining to the power-electronics-based subsystem (e.g. HVDC, UPFC) with the power flow equations of the main system. This set of equations may then be solved using standard approaches such as NR, thus solving simultaneously the equations of the subsystem and the main system. Therefore, the impact of the subsystem's internal equations on the terminal voltages and their relation with the rest of the system is properly included in the solution procedure. However, the integration of new components in existing solvers is not always feasible or desirable due to the complexities and costs associated with reprogramming already developed packages. Hence, a sequential solution approach has been developed, as explained next.

Sequential Solution

The sequential approach considers the main system and the intended subsystem sequentially in the power flow solution procedure. In other words, starting from an initial state for the system, the main system is solved assuming that voltages and flows at the subsystem's terminals are set at their initial values. The subsystem is then solved using the computed system values at its terminals, checking for any subsystem limit violations; its terminal voltages and flows are then modified to resolve any violations, if necessary, before passing the results back to the main system solution routine. This procedure is iterated until the error on the subsystem terminal values between two consecutive iterations becomes smaller than a pre-specified threshold.

The convergence characteristics of sequential and unified approaches are almost identical if the main system is strong with stiff voltage magnitudes [27]. However, for weak systems, convergence of sequential methods is problematic. Thus, the performance of the sequential solution method relies on the behavior of terminal voltages that link the subsystem's internal equations to those of the main system. In this case, adequate techniques to address this issue should be developed, so that the sequential method is made more reliable.

2.3 Optimal Power Flow

The economic operation of power systems can be achieved using an OPF approach, with operating costs being minimized as an objective function [28]. This framework can also be used to determine the optimal ratings/locations of new installations during design and planning studies.

System operational and security constraints as well as operating limits are usually included in a "standard" OPF formulation, which mathematically may be stated as follows

[26]:

$$\min \quad Costs = \sum_{k \in \mathcal{G}} C_k \left(P_{Gk} \right) \tag{2.5a}$$

$$\text{s.t.} \quad F(\delta, V, Q_G, P_G, P_D, Q_D) = 0 \tag{2.5b}$$

$$H(\delta, V, Q_G, P_G, P_D, Q_D) \leq 0 \tag{2.5c}$$

$$P_{Gk\,\min} \leq P_{Gk} \leq P_{Gk\,\max} \qquad \forall k \in \mathcal{G} \tag{2.5d}$$

$$Q_{Gk\,\min} \leq Q_{Gk} \leq Q_{Gk\,\max} \qquad \forall k \in \mathcal{G} \tag{2.5e}$$

$$V_{k\,\min} \leq V_k \leq V_{k\,\max} \qquad \forall k \in \mathcal{N} \tag{2.5f}$$

where $C_k(\cdot)$ stands for the generator k production cost, which is typically a piecewise-linear quadratic function; $F(\cdot)$ corresponds to the network power flow equations and other equality constraints used to model embedded systems such as FACTS controllers; $H(\cdot)$ represents transmission system limits, such as line flow limits, and other limits of embedded components; $\mathcal{N}$ and $\mathcal{G}$ stand for the set of all buses and generators, respectively; P_D and Q_D correspond to the active and reactive power demand; P_G and Q_G represent the active and reactive powers of generators; and V and δ are the bus voltage phasor magnitudes and angles.

The objective function and/or constraints are nonlinear. Thus, the OPF formulation is a nonlinear problem, requiring nonlinear programming (NLP) methods for its solution. These types of problems are inherently difficult to solve, because:

- An optimum is not necessarily at the edge of a feasible region (unlike linear programming), and can be anywhere in the feasible region.
- The feasible region may be discontinuous, with multiple parts, which complicates the solution process.
- It is usually not possible to find a global optimum, so that the solution is usually a local optimum. Hence, different starting points may lead to different final solutions. For example, the problem might seem to be infeasible when starting from a given initial point, even though there may be actually a solution.

There are few software packages available with robust solvers to solve large NLP problems, such as AMPL and GAMS [29], [30]. The software package for solving optimization problems used in this work is AMPL, which is an algebraic modeling language for linear and nonlinear optimization problems, using the Knitro solver [29].

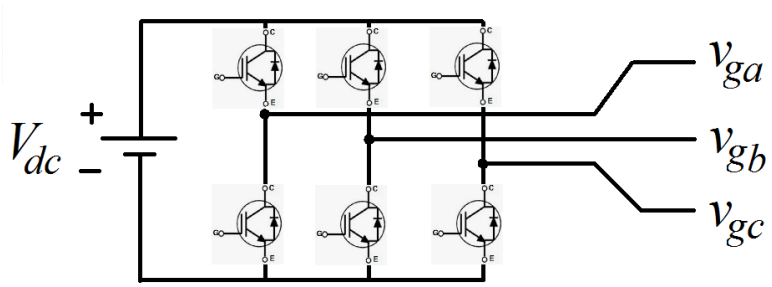

Figure 2.2: Simple diagram of a VSC with bi-directional switches.

2.4 Voltage Source Converters

A VSC is shown in Figure 2.2 in its basic form, comprising six bi-directional switch elements composed of an IGBT and an anti-parallel diode, which are typically turned on/off based on carrier and modulating signals in a Pulse Width Modulating (PWM) approach to yield a desired voltage at the converter output. The PWM switching frequency w_s is high enough to facilitate filtering while limiting losses and noise interference.

2.4.1 Pulse Width Modulation (PWM)

The converter operates with alternatively connecting and disconnecting the switches on the same leg creating a square-shape waveform at the output v_{ga}, using ON/OFF commands for these switches obtained from a PWM strategy [31]. In other words, the reference signal is compared with a high-frequency periodic triangular signal called carrier signal; the intersections of these two signals determine the switching instances of the converter switches. The frequency of the carrier signal should be significantly greater than the rate of change in the reference signal.

2.4.2 Harmonic Filter

The output voltage of the converter before the filters changes rapidly between $+V_{dc}/2$ and $-V_{dc}/2$ (or 0 and V_{dc} depending on the reference), and is hence not the sinusoidal waveform that a power system requires. Hence, a harmonic filter, which includes the inductance of the transformer at the converter output, is used to eliminate most of the high-frequency harmonic contents and deliver a waveform close to a sinusoidal at the network terminals.

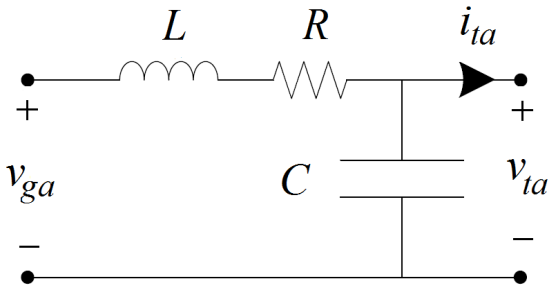

Figure 2.3: LC harmonic filter.

A simple LC filter for Phase a, for example, is shown in Figure 2.3, where v_{ga} is generated by the switches and v_{ta} is the filtered output. The filter's capacitor is not essential, but, it is useful to decrease the harmonic contents of the output current.

It is important to note that the filter affects the fundamental harmonic as well, and thus its impact on the output voltage and current should be considered. The filter is designed based on the output rating and ripple requirements as well as the switching frequency. Hence, according to a basic design procedure outlined in [32], the inductor L is calculated to limit the maximum current ripple, while assuring that the voltage drop does not exceed a threshold (e.g. 5% of the rated voltage), as follows:

$$\Delta I_{\max} = \frac{V_{dc}/3}{4Lf_s} \tag{2.6}$$

where $f_s = w_s/(2\pi)$ is the switching frequency. The capacitor C, if used, is obtained based on the switching frequency as follows:

$$C = \frac{1}{L\left(2\pi f_r\right)^2} \tag{2.7}$$

where f_r is the resonance frequency of the filter, and can be assumed to be a decade lower than f_s. The resistor R mainly represents the controller losses, including transformers, which should not exceed 2% of the converter rated power.

2.5 HPFC

The architecture of a typical installation of the HPFC is shown in Figure 2.4 [9]. The core of the device is a variable shunt susceptance accompanied by two converters and their

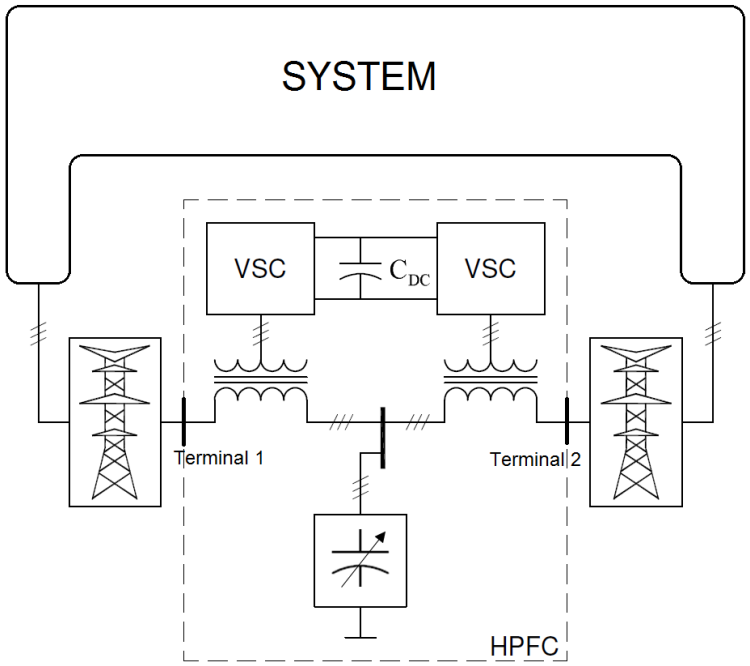

Figure 2.4: The HPFC Architecture.

transformers. In this figure, the shunt device can be an SVC or a passive (switchable) capacitor bank. The converters share a common DC link to exchange active power. If the active power loss inside the device is ignored, its net exchange of active power with the system is zero. The converter outputs as well as the shunt susceptance are changed to regulate the power flow through the associated line, and consequently the power exchange between the two line terminals. If there is another corridor between the two line terminals, parallel to the one with the HPFC, the power flow through that corridor can be controlled indirectly using this device. The HPFC can also be used to regulate its terminal voltages. Power and voltage regulation is feasible as long as the device stays within its capability limits.

The controller is assumed to be lossless, which is equivalent to a constant voltage for the dc link; however, the current references can be slightly altered to account for the losses. Therefore, the loss can be addressed separately by the dc voltage control loop without loss of generality. The sum of active powers generated by the converters, given that the internal losses are neglected, should be zero, which dictates a zero net active power exchange between the device terminals and the grid [20]. This approximation removes the

need for a separate iterative loop in simulation studies [19].

2.6 Software Packages

There are several commercially available software packages that can be used for the power system analyses required in this research work. The tools used in this research are described next.

2.6.1 PSAT

The Power System Analysis Toolbox (PSAT) is a MATLAB-based software package for power system analysis [33], [34]. The main components and features of PSAT are:

- Power flow.
- Continuation power flow
- Optimal power flow.
- Small signal stability analysis.
- Time domain simulation.
- A graphical user interface.
- User defined models.
- FACTS models.
- Wind turbine models.
- Conversion of data files from several Formats.
- Export results to different formats; interfaces to GAMS and UWPFLOW programs [35].
- Command line interface.

This toolbox is freely available under a public license, which makes it a useful tool for researchers and educators. The toolbox model library is quite comprehensive and includes most of the components required for power system studies. However, the main advantage of this package is that its source code is open for modification. Moreover, it is based on MATLAB, so that most of the familiar and powerful MATLAB-coding tools and toolboxes can be used in conjunction with PSAT for power system analysis.

2.6.2 PSS®E

PSS®E is a popular power system analysis software from SIMENS Energy Inc. [25]. It can be used for the following planning and operation studies:

- Power flow.
- OPF.
- Balanced or unbalanced fault analysis.
- Dynamic simulation.
- Market tools.
- Transfer limit analysis.
- Network reduction.

This software is popular in industry, with many system operators using this package as their standard analysis tool.

2.6.3 AMPL

AMPL offers a text-based environment that can be used to solve optimization problems efficiently [29]. This software package integrates a modeling language for describing optimization data, variables, objectives, and constraints, and provides a command language for debugging models and analyzing results. It uses packaged solvers to find a feasible solution for the optimization model. These solvers can accommodate a variety of problems with different mathematical models including linear, non-linear, mixed-integer, and etc.

The Knitro solver is used in this work, which is primarily designed for finding local optimal solutions of large-scale, continuous nonlinear problems [36]. In general, it can be used to solve all of the following classes of optimization problems:

- Unconstrained.
- Constrained.
- Linear programming problems (LPs).
- Systems of nonlinear equations.
- Mixed integer problems.
- Models with complementarity constraints.

This solver mostly uses interior point methods for solving nonlinear optimization problems. However, there are two other main solution methods that Knitro can use, namely, Sequential Quadratic Programming (SQP) and the branch and bound algorithms; the latter is used to solve mixed integer problems. It is interesting to note that the inclusion of complementarity constraints in an optimization model for power system studies is important, since reactive power limits of generators may be modeled using these types of constraints in certain OPF models [37]. The AMPL software package is not completely free of charge, but it can be obtained and used at a very low price for academic and research purposes.

2.6.4 PSCAD™/EMTDC™

The EMTDC (Electromagnetic Transients including DC) software allows to model and solve differential equations for electromagnetic and electromechanical systems in the time domain [15]. Solutions are calculated based on a fixed time step, and its program structure allows for the representation of control systems. The simulator is wrapped in a graphical user interface and is referred to as PSCAD, which allows the user to graphically assemble the circuit, run the simulation, analyze the results, and manage the data in an integrated graphical environment. Studies that can be conducted using PSCAD/EMTDC include:

- Contingency studies of AC networks and its components.
- Control system design and modeling of FACTS and HVDC systems.
- Insulation coordination of transformers, breakers and arrestors.
- Relay coordination.

2.7 Summary

Relevant concepts, methods, and tools required for this research work were reviewed in this chapter. First, a general overview of the modeling approach used here and its different stages based on the intended application and target software package were presented. Next, the basics of steady-state power system analyses, namely, power flow and OPF, were discussed; the integration of FACTS controllers into these analysis techniques was also discussed, highlighting some related computational implications. Then, a simple architecture of the VSC with its main components, i.e. switches, filter, and typical control approaches were reviewed before providing a general overview of the HPFC. Finally, several relevant software packages used in the research work were also briefly described.

Chapter 3

HPFC Power Flow Modeling

This chapter presents and discusses the power flow model of the HPFC developed for steady-state studies of power systems, and presents and discusses the results obtained when applying this model. The numerical studies presented here are carried out using a two-area benchmark system as well as a detailed model of the Ontario-Canada grid, showing the effectiveness of the controller in regulating power system variables.

3.1 Model and Control

Power flow solutions for a power system provide essential steady-state information on the phasor voltages and power flows in the system, with all existing components being represented and included in the calculations. The HPFC is included sequentially in the power flow calculations presented here, to insure that its operating limits are properly represented without compromising the power flow performance, as discussed in Section 2.2. The flow chart of the intended power flow studies is illustrated in Figure 3.1. It starts from an initial known solution for the grid, which is used to solve the system using PSS®E's solver, assuming that voltages and flows at the HPFC terminals are set at their initial values. The equations for the controller are then solved using the computed system values at its terminals, checking for any internal limit violations. The terminal voltages and flows are then modified to relieve any violations and define the controller operating mode, if necessary, before passing the results back to the main system solution routine; this is carried out here using a custom Python code [38]. This procedure is iterated until the error on the HPFC terminal values between two consecutive iterations becomes smaller than a pre-specified threshold. Finally, the results are reported so that the impact of the HPFC

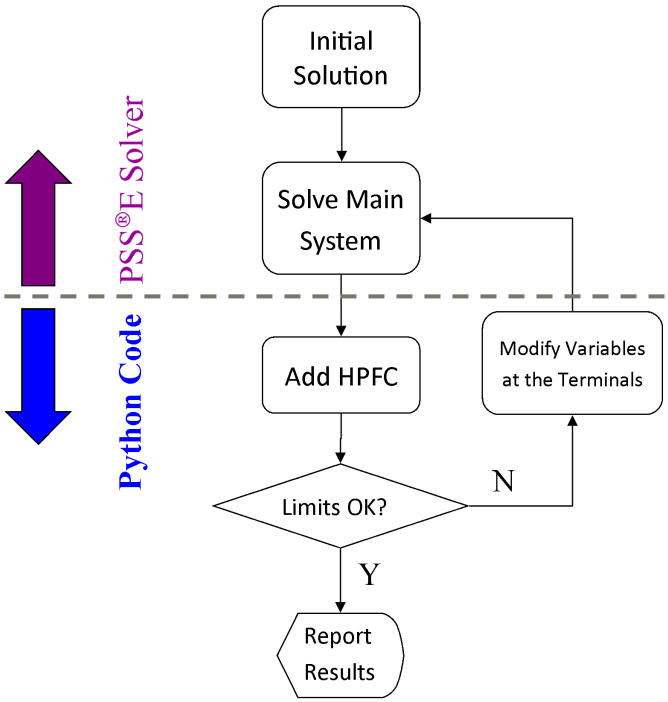

Figure 3.1: Power flow solution procedure for the Ontario grid with the HPFC.

on the system can be analyzed. The implementation of this approach is explained in detail in [39].

Figure 3.2 shows the equivalent circuit model for the HPFC in a two-area system. A variable shunt susceptance with two series voltage sources represent the main components of the device. Voltage phasors $\boldsymbol{V}_1$ and $\boldsymbol{V}_2$ represent the device terminals (1 and 2) which are connected to the associated system. The two areas are represented by their Thevenin equivalents at the device terminals; the leakage reactances of the controller series transformers are included in the equivalent Thevenin impedances.

Four modes for controlling the device are possible, i.e. PVV, PQQ, V, and Z as per Figure 3.3. The topology of the device is the same in PVV and PQQ modes. In the PVV mode, setpoints for P, V_1, and V_2 values are defined, while in the PQQ mode the P, Q_1, and Q_2 values are defined. It is important to note that when the device limits are reached and it is in the PQQ mode, the values of P, Q_1, and Q_2 are obtained by the limit handling strategy discussed later and are not known beforehand.

In the V mode, the powers cannot be regulated because of the device limits being

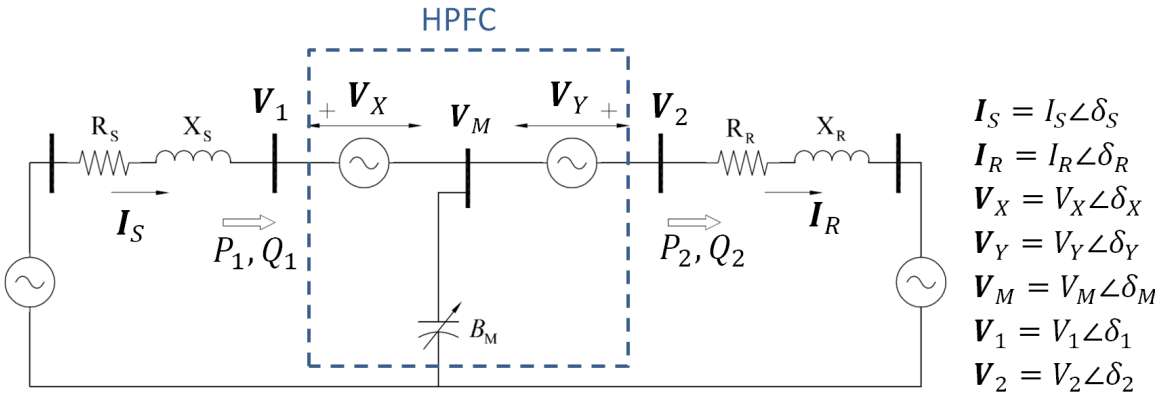

Figure 3.2: Circuit model for the HPFC in a system.

reached, and the device turns into a shunt voltage regulator with the two series voltage sources bypassed. The voltage setpoint in the V mode can be assumed to be the same value as in the PVV mode, if both terminals were set to identical values, with the voltage regulation being achieved by changing the variable shunt susceptance. This shunt susceptance may reach its limit at certain power transfer level; therefore, the device at that point is seen by the network as a fixed shunt, and is thus referred here as the Z mode. Observe that in V and Z modes, $V_1 = V_2 = V_M$ and $V_X = V_Y = 0$.

The main operating limits of the device need to be considered on the following variables and parameters, as per Figure 3.2:

- The device main current magnitudes: I_S and I_R.
- Inverter voltage magnitudes: V_X and V_Y.
- Shunt device voltage and susceptance magnitudes: V_M and B_M.

In practical cases, the maximum allowable values for V_X and V_Y is small (e.g. 0.05 p.u.), to keep the inverter rating and price as low as possible. Thus, the limit for $V_M = |\boldsymbol{V}_M| = |\boldsymbol{V}_1 - \boldsymbol{V}_X| = |\boldsymbol{V}_2 - \boldsymbol{V}_Y|$ is dependent on the terminal voltages $\boldsymbol{V}_1$ and $\boldsymbol{V}_2$. Note that the currents flowing through the series branches ($\boldsymbol{I}_S$ and $\boldsymbol{I}_R$) and their magnitude limits are handled directly without the need to deal with other parameters, including small transformer impedances, which is known to cause numerical instabilities [1]. The limit control strategy for I_S, I_R, V_X, V_Y and B_M is explained next.

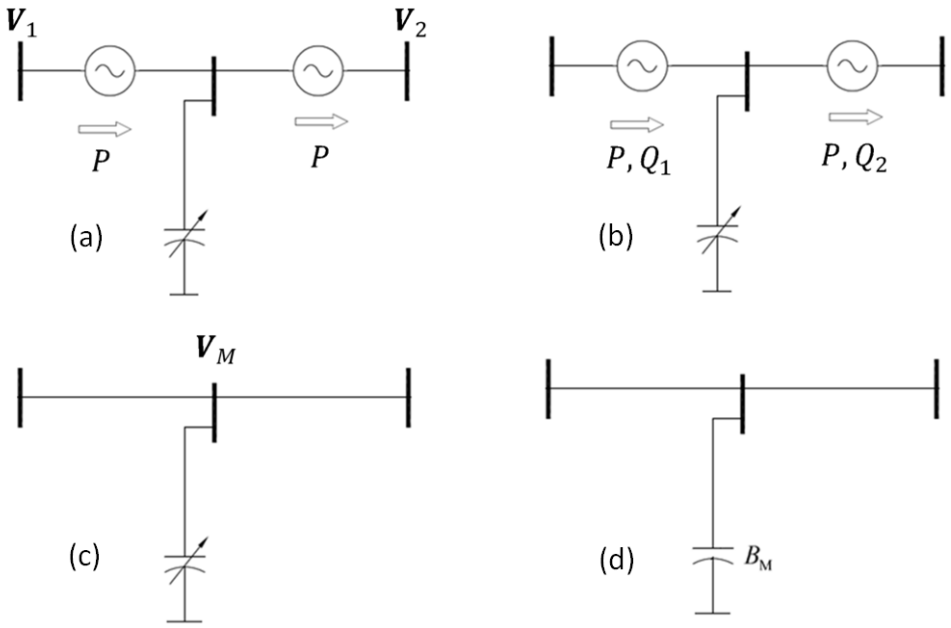

Figure 3.3: Four control modes of the HPFC: (a) PVV, (b) PQQ, (c) V, and (d) Z.

There are four control modes for the HPFC, as previously mentioned, with the default control mode being the PVV mode, in which the active power flow and the voltage magnitudes at the device terminals are independently controlled. However, based on the system conditions and the device operating limits, the HPFC may have to switch to other control modes, with the device operating constraints increasingly being relaxed as it moves from PVV to PQQ, to V, and finally to Z control.

The transitions between its four control modes are shown in Figure 3.4. The device usually starts operating in the PVV mode, where setpoints for P, V_1, and V_2 are defined. If the device reaches its limits on at least one the main variables, i.e. I_S, I_R, V_X, or V_Y, the controller switches to PQQ mode, in which setpoints for P, Q_1, and Q_2 are defined to resolve the limit violation, so that these values are close to those corresponding to the PVV mode, as explained in Section 3.1.2. The HPFC continues operating in the PQQ mode until the limit violations cannot be resolved by the modification of the P, Q_1, and Q_2 setpoints, at which point the device switches to V mode. The control modes PVV and PQQ are closely related, since the device topology is the same in these two modes.

In the V mode, the two series voltage sources in Figure 3.2 are bypassed, and the voltage magnitude at the shunt bus V_M is regulated at a given level by using the variable shunt

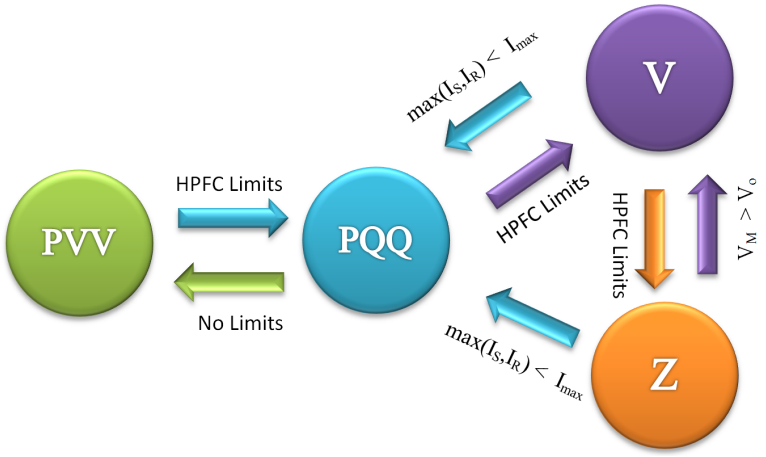

Figure 3.4: Transitions between the four HPFC control modes.

susceptance B_M; in this mode, $V_1 = V_2 = V_M$, so that the terminal voltages are considered to be regulated as well. This voltage regulation is feasible as long as the shunt device is capable of providing the required B_M value, but this is not always possible because of the limited shunt device capability, at which point B_M is fixed and the device switches to Z mode. In this mode, the device has its minimum regulation capability and behaves as a passive fixed shunt susceptance in the system.

The path from the PVV mode through PQQ, V, and Z modes can be associated with a gradual increase in the HPFC loading. In this case, the device responds to the higher demand by relaxing more operating constraints to avoid exceeding the device ratings. However, a recovery is also possible when the loading level allows and stricter regulation becomes feasible. For instance, the device may switch to PQQ mode from V or Z modes if the largest current flowing through the series branches is below the corresponding inverter limit. Similarly, in Z mode, if the voltage recovers, the control switches to V mode. The HPFC is always initialized for power flow studies in PVV mode by default. This mode switching logic is explained in detail next.

3.1.1 PVV Mode

In this mode, the device is assumed to regulate the active power flow and the terminal voltages at a given level; this is feasible as long as the device stays within its capability limits. Figure 3.5 shows the flowchart of the control strategy; in the case of a limit violation

that is not relieved by changing B_M (see Section 3.1.2), the device is assumed to switch to the PQQ mode, so that the limit violations can be resolved in the new mode. In the case of a non-convergent power flow, the control mode is switched to V mode, which is a conservative approach that considers all possible scenarios before declaring a true non-convergent power flow.

3.1.2 PQQ Mode

The proposed strategy for the PQQ mode tries to keep currents and voltages at the same time away from their limits. The approach is based on the sensitivity of the device power injections with respect to its internal voltage and current magnitudes. In this strategy, B_M can be considered to be a discrete parameter. The flowchart of the proposed strategy is illustrated in Figure 3.6, showing how the internal voltages and currents are modified to bring the device within its limits; this is accomplished using the sensitivity analysis explained next. It is critical to start with a reasonable value for the shunt device susceptance B_M; thus, a proper value should be choosen first, as discussed later.

New values for P, Q_1, and Q_2 are calculated using a sensitivity matrix G and the magnitude of the limit violation. These new values are used to run a power flow, which if it converges, the results are checked for any limit violation; otherwise, the incremental step is halved, and the power flow analysis is repeated. This procedure is iterated a few times (e.g. $m_{max} = 2$) until convergence is achieved; limit violations are also checked iteratively for a few iterations (e.g. $n_{max} = 2$). In either of these loops, if the maximum iteration number is reached without achieving convergence or resolving the limit violation, the control mode is switched to V mode to relax power regulation; otherwise, the final results are displayed.

PQQ Setpoint Calculation

The desired P, Q_1, and Q_2 values and the sensitivity matrix G are determined as follows: From Figure 3.2, P, Q_1, and Q_2 can be obtained as follows:

$$P = Re\left\{\left(\boldsymbol{V}_Y + \boldsymbol{V}_M\right)\boldsymbol{I}_R^*\right\} \tag{3.1}$$

$$Q_1 = Im\left\{\left(\boldsymbol{V}_X + \boldsymbol{V}_M\right)\boldsymbol{I}_S^*\right\} \tag{3.2}$$

$$Q_2 = Im\left\{\left(\boldsymbol{V}_Y + \boldsymbol{V}_M\right)\boldsymbol{I}_R^*\right\} \tag{3.3}$$

$$\boldsymbol{V}_M = \frac{\boldsymbol{I}_S - \boldsymbol{I}_R}{jB_M} \tag{3.4}$$

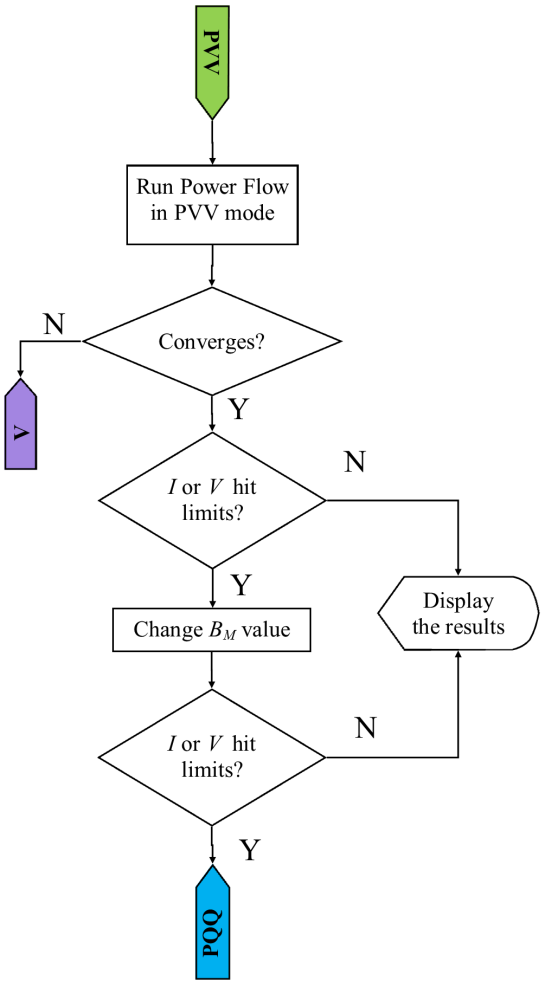

Figure 3.5: Control strategy in PVV mode.

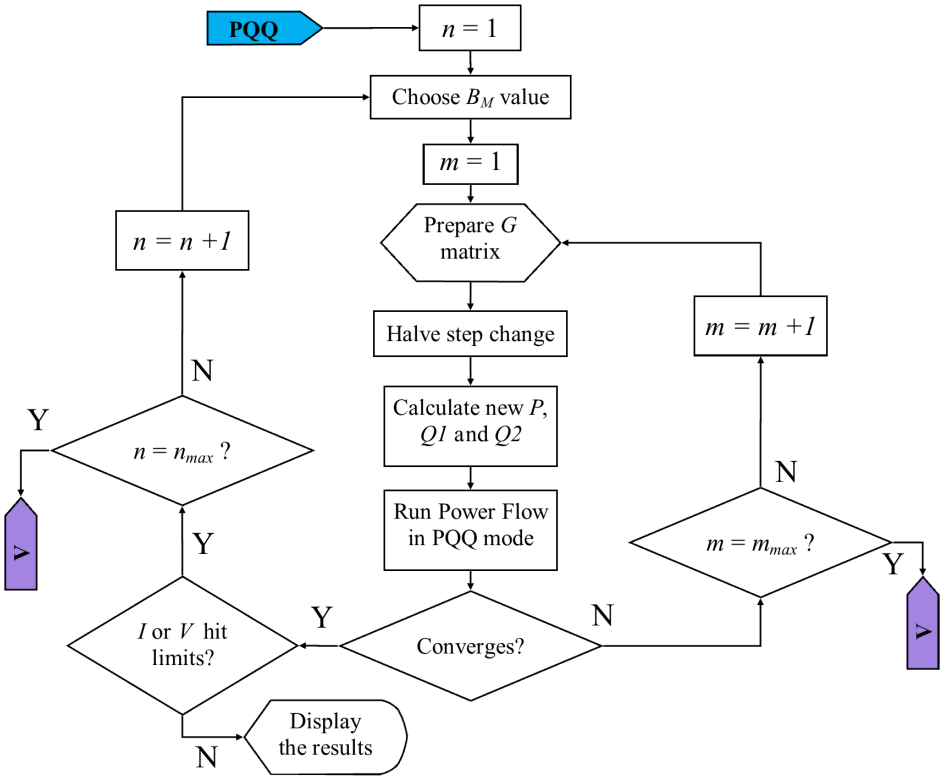

Figure 3.6: Control strategy in PQQ mode.

Therefore, their derivatives can be obtained, assuming that the devices terminal voltages are stiff, and the matrix G can be defined as:

$$G = \begin{bmatrix} \frac{\partial P}{\partial I_S} & \frac{\partial P}{\partial I_R} & \frac{\partial P}{\partial V_X} & \frac{\partial P}{\partial V_Y} \\ \frac{\partial Q_1}{\partial I_S} & \frac{\partial Q_1}{\partial I_R} & \frac{\partial Q_1}{\partial V_X} & \frac{\partial Q_1}{\partial V_Y} \\ \frac{\partial Q_2}{\partial I_S} & \frac{\partial Q_2}{\partial I_R} & \frac{\partial Q_2}{\partial V_X} & \frac{\partial Q_2}{\partial V_Y} \end{bmatrix} \tag{3.5}$$

Based on G, the power changes can be calculated as follows:

$$\begin{bmatrix} \Delta P \\ \Delta Q_1 \\ \Delta Q_2 \end{bmatrix} = K^m G \begin{bmatrix} \min\left(0, (I_{Smax} - I_{So})\right) \\ \min\left(0, (I_{Rmax} - I_{Ro})\right) \\ \min\left(0, (V_{Xmax} - V_{Xo})\right) \\ \min\left(0, (V_{Ymax} - V_{Yo})\right) \end{bmatrix} \tag{3.6}$$

$$\begin{bmatrix} P \\ Q_1 \\ Q_2 \end{bmatrix} = \begin{bmatrix} P_o \\ Q_{1o} \\ Q_{2o} \end{bmatrix} + \begin{bmatrix} \Delta P \\ \Delta Q_1 \\ \Delta Q_2 \end{bmatrix} \tag{3.7}$$

where $_o$ refers to the starting values of all required variables, and the factor K has a value of 0.5 in the iterative process, with m representing the loop counter in Figure 3.6.

Improved Sensitivity Matrix

The derivatives in the previous section were obtained assuming that the internal variables are isolated from the rest of the system; in other words, the power flow equations of the rest of the system were ignored, which under stressed conditions is not true. However, the maximum allowable values for V_X and V_Y are usually small (e.g. 0.05 p.u.), and these variables are quite sensitive to changes in the terminal voltages. Therefore, using the technique presented in the previous section may lead to convergence problems, especially when the system is stressed. Thus, G can be improved by using derivatives with respect to V_X and V_Y that considers voltage changes at the device terminals, since one can demonstrate that $dV_X \approx dV_1$ and $dV_2 \approx dV_2$. Hence, in (3.5):

$$\frac{\partial P}{\partial V_X} = \alpha \frac{\partial P}{\partial V_1} \tag{3.8}$$

$$\frac{\partial P}{\partial V_Y} = \alpha \frac{\partial P}{\partial V_2} \tag{3.9}$$

and similarly for the corresponding Q_1 and Q_2 derivatives. In (3.8) and (3.9), α is a scalar (e.g. $\alpha = 0.5$) introduced to further reduce the step in the iterative procedure presented in Figure 3.6, and thus improve convergence.

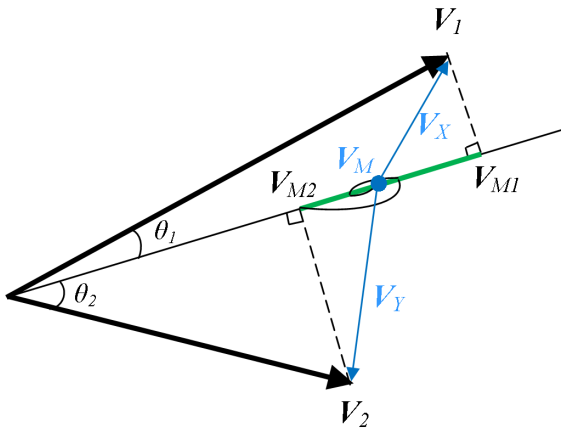

Figure 3.7: Voltage phasor diagram.

Choosing the B_M Value

The voltage magnitude on the inverters outputs depends on the shunt device voltage and thus the value of B_M. Therefore, a "good" B_M value facilitates relieving the voltage limit violations. This is the first step depicted in Figure 3.6 before the iterative procedure described previously. The procedure to determine B_M value is explained next.

Based on the terminals voltages available from a previous power flow solution, an approximate working guess of V_M (and B_M) can be obtained as follows: Figure 3.7 depicts an exaggerated diagram of the voltage phasors. The smallest values for V_X and V_Y are achieved when $\boldsymbol{V}_M$ lies between $\boldsymbol{V}_{M1}$ and $\boldsymbol{V}_{M2}$. Therefore, to have $\boldsymbol{V}_M$ within this interval or close to it, first $\boldsymbol{V}_{M1}$ and/or $\boldsymbol{V}_{M2}$ are obtained using an initial guess for B_M to see if these yield feasible V_X and V_Y; if not, the interval between $\boldsymbol{V}_{M1}$ and $\boldsymbol{V}_{M2}$ is halved, with the resulting $\boldsymbol{V}_M$ yielding new $\boldsymbol{V}_X$ and/or $\boldsymbol{V}_Y$ phasors. If these $\boldsymbol{V}_X$ and/or $\boldsymbol{V}_Y$ are within their magnitude limits, then the associated value of B_M is computed; otherwise, the algorithm continues bisecting the interval until a feasible result, if it exists, is obtained, or a certain maximum iteration number (e.g. 3) is reached. The minimum $V_X + V_Y$ is used to choose the direction while halving the interval. The desired B_M value is calculated based on the obtained value for V_M; for discrete values of the shunt device, the closest step to the calculated value is chosen and used in the next step.

3.1.3 V Mode

In this mode, the two series voltage sources (see Figure 3.2) are bypassed and $V_1 = V_2 = V_M$. The voltage magnitude at the terminals are regulated at a given level using the variable shunt susceptance B_M, with no active power flow control by the device. Thus, the power flow is run assuming the device terminals and the shunt bus merged into one bus with a regulated voltage magnitude. As shown in Figure 3.8, if the power flow does not converge, the control mode switches to Z mode; otherwise, the largest of the input and the output currents (I_S and I_R) are checked with respect to the inverters current limits. If it is within the limits, the device recovers and switches to PQQ mode; otherwise, based on the reactive power injection at the shunt bus obtained from the power flow analysis, the required B_M value is calculated. Since the shunt device has a maximum limit, if the calculated B_M exceeds this value, the shunt susceptance is fixed at B_{Mmax}, and the control mode is switched to Z mode. Otherwise, the control remains at V mode and final results are displayed. Note that if B_M is discrete, the voltage setpoint in the V mode will vary accordingly.

3.1.4 Z Mode

The Z mode corresponds to the HPFC at its minimum regulating capability. The B_M in this case is fixed at its maximum value and $V_1 = V_2 = V_M$, and thus the device can be represented as a passive fixed shunt susceptance in power flow analyses as illustrated in Figure 3.9.

3.2 Results and discussions

The results of applying the discussed HPFC model to address congestion problems in a two-area benchmark test system and in the Ontario-Canada grid are presented in this section. In these studies, the power setpoints are varied and the voltage setpoints are chosen to be the same or very close to the values corresponding to the base-case conditions. This approach provides a meaningful and yet simple template to study and compare the power flow results without and with the added HPFC. The power flow studies of the two-area system are performed using PSAT [33] and PSS®E [25]. The power flow studies of the Ontario system are carried out using PSS®E. The detailed power flow model is integrated into the standard PSS®E solver using a custom Python code [38], which was used to

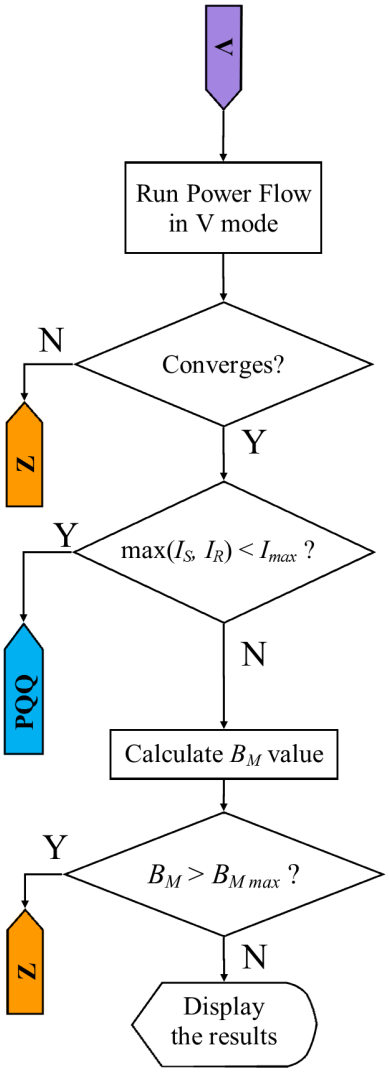

Figure 3.8: Control strategy in V mode.

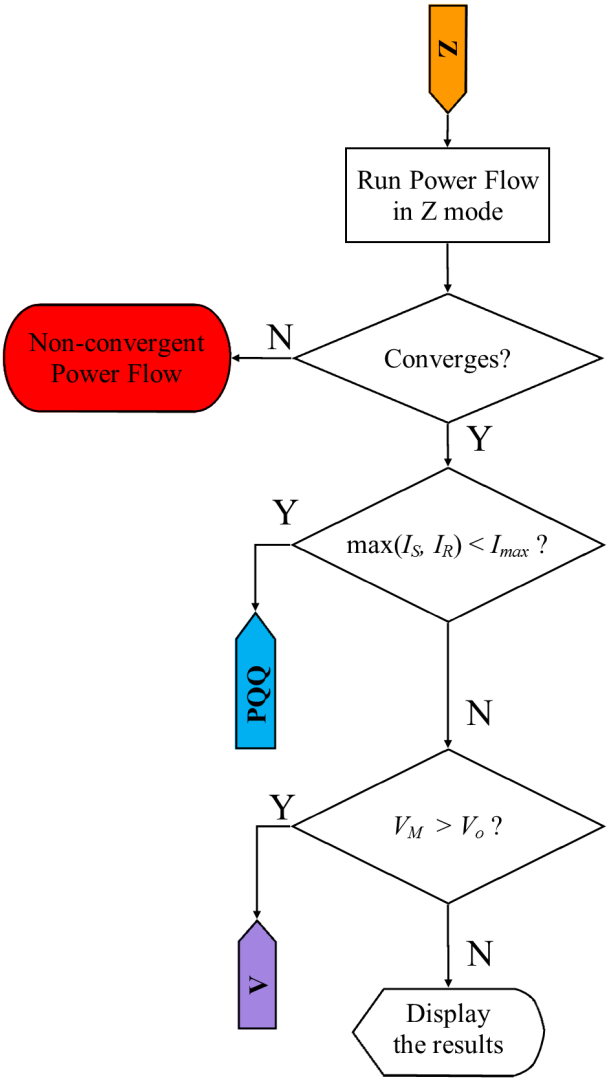

Figure 3.9: Control strategy in Z mode.

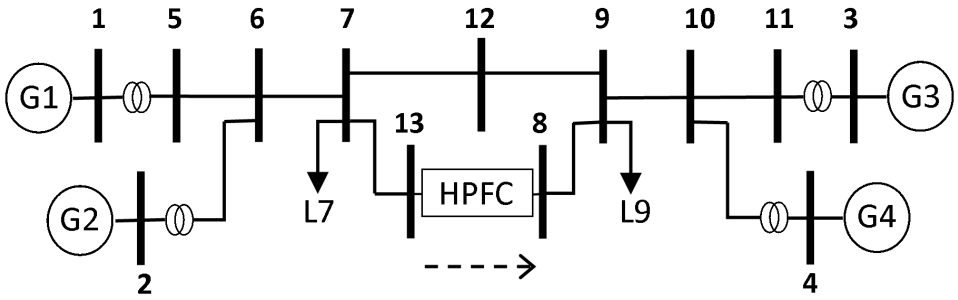

Figure 3.10: Two-area test system.

introduce the mathematical model and procedure required to represent the HPFC within PSS®E, as explained at the beginning of Chapter 3.

3.2.1 Two-area Test System

A modified version of Kundur's two-area test system is used here [40]. The system is loosely based on the Ontario network, representing the main generators, loads, and east-west system interconnections. Figure 3.10 shows the single-line diagram of the system, and the associated data can be found in Appendix A. The system was chosen because it is composed of two areas connected by a tie-line with two corridors, which can be readily used to demonstrate and study the application of the HPFC.

The HPFC is connected between Bus 13 and Bus 8 in the lower corridor. The controller is assumed to start in PVV mode, i.e. with three setpoint values for its active power flow and the voltage magnitudes at its terminals. The voltage magnitudes of the system before introducing the HPFC are used here as the setpoints without loss of generality; note that the setpoints can be set arbitrarily as desired by the operator or based on a chosen dispatch policy.

Loadability studies are performed assuming Bus 9 and Bus 2 as a power sink and a source, respectively, to analyze the impact of the HPFC on the test system. Thus, the power transfer between these two nodes is increased until the power flow cannot be solved, gradually increasing the load in 0.1 p.u. steps. The required HPFC parameters used here are the following:

- Maximum current magnitudes (I_S and I_R): 2 p.u.

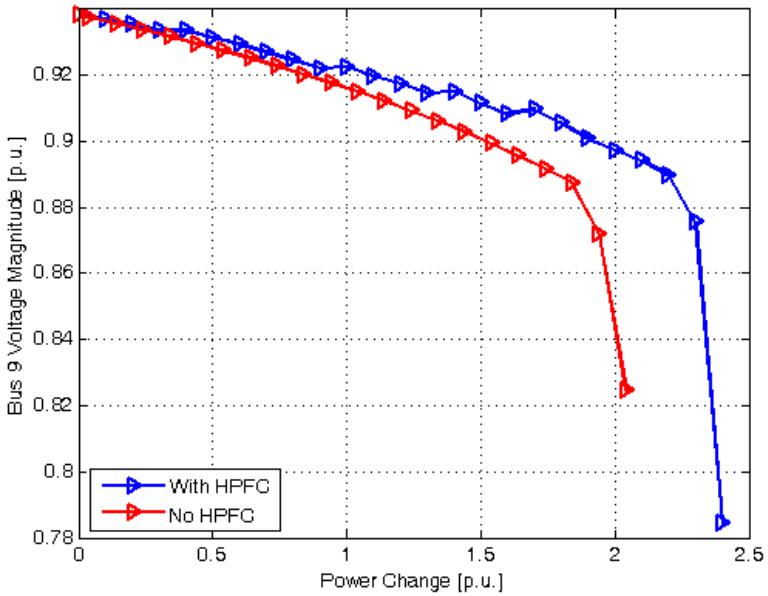

Figure 3.11: PV curves at Bus 9 of the two-area system with and without HPFC.

- Maximum voltage magnitude for the converters including transformers (V_X and V_Y): 0.04 p.u. (9.2 kV).
- Discrete shunt susceptance with four equal steps (0.2 p.u. each): $0 \leq B_M \leq 0.8$ p.u.
- Active power share of the lower corridor with respect to the total tie-line flow: 25%.
- Voltage magnitude setpoint at the terminals: 0.9557 p.u.

The maximum loadability of the system at Bus 9 increases from 2.04 p.u. (204 MW) to 2.4 p.u. (240 MW), i.e. almost 20%, when introducing the HPFC. In this study, the sensitivity matrix G is determined based on the procedure discussed in Section 3.1.2. The voltage profile at the sink Bus 9 is depicted in Figure 3.11, with and without the HPFC; observe that the HPFC improves the maximum loadability and voltage profile.

The HPFC control modes and B_M values at different operating points are shown in Figure 3.12. Note that the device starts in the PVV mode, and switches to different modes according to the system requirements at different operating points as the load increases. At the last four operating points, the HPFC has exhausted its capability limits

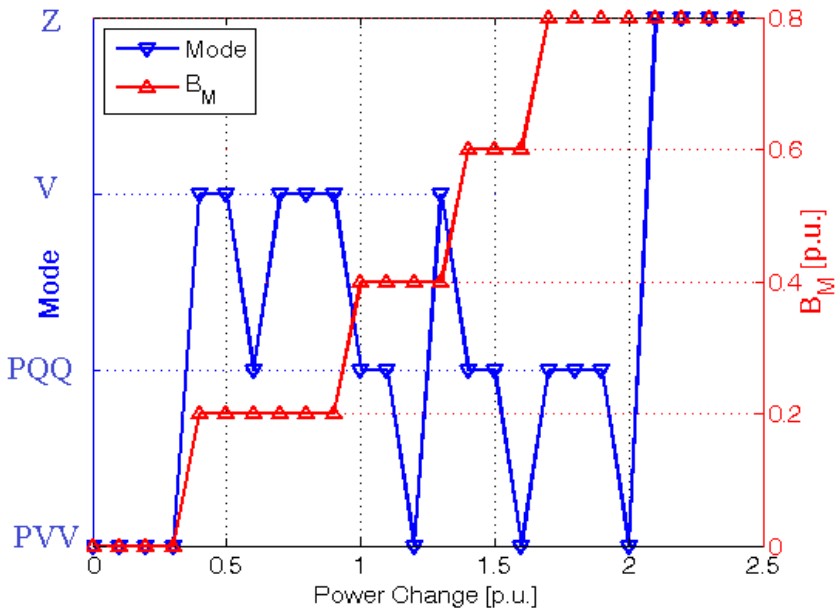

Figure 3.12: HPFC control modes and B_M as the loading level increases for the two-area system.

and thus behaves as a fixed shunt susceptance in the Z mode. Observe that the algorithm transitions to the best feasible mode using the available shunt susceptance steps, based on the procedures depicted in Figures 3.5–3.9.

Figure 3.13 shows the active powers flowing through the lower and upper corridors between the two areas, as well as their sum. Note that the HPFC is installed on the lower corridor, thus controlling the power transfer in the corresponding line according to the chosen setpoint.

3.2.2 Application to Ontario-Canada's Grid

A detailed model of the Ontario-Canada system is used here to examine the use of the HPFC model within a realistically large system, motivated by the interest in and relevance of these studies to Ontario's Hydro One and Independent Electricity System Operator (IESO), who provided input for these studies. The prospective HPFC installation would provide system operators with the ability to control the flows and adequately regulate the voltage profile in the grid, thus providing congestion relief at peak-demand and voltage

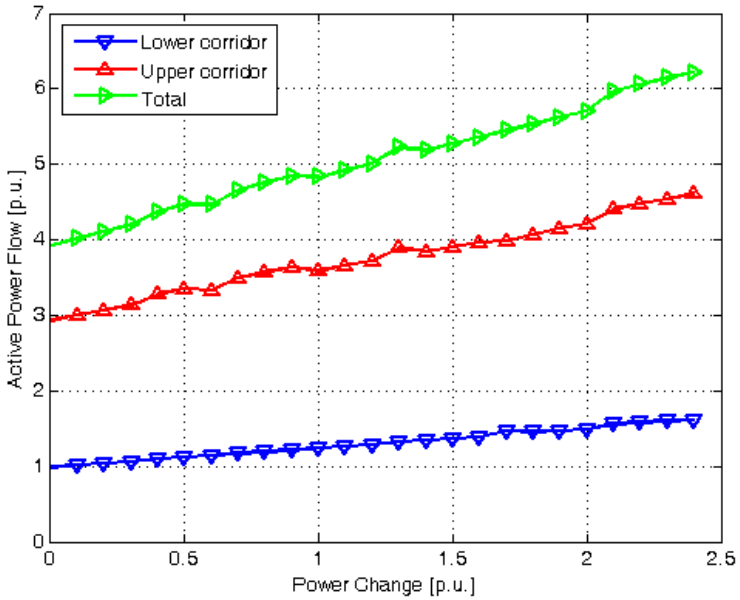

Figure 3.13: Active power flow in the tie-line corridors connecting the two areas of the test system.

support in the case of contingencies. Therefore, the performance of the HPFC under realistic conditions and scenarios are studied here, and the results are presented and discussed next.

Network Model

The base-case dataset for the grid was obtained from the IESO, and contains information for a power flow solution at a peak demand period [41]. It spans the power network from New Brunswick to Kentucky, including Ontario, New York, and areas in between. It has 6895 buses, 38085 branches, 1890 generator units, and a total load of 267 GW.

Potential HPFC Locations

Based on the input from the IESO, the following four locations on the Ontario grid were studied for the potential HPFC installation, given that the associated lines are prone to congestion problems discussed in Appendix B:

a. A 115 kV double-circuit in the Ottawa region.

b. A 115 kV double-circuit in Bell River.

c. A 115 kV double-circuit in the Burlington area.

d. Two 220 kV double-circuits around Trafalgar supplying Toronto, the main load center of the province.

The approximate locations of these lines are marked on the provincial grid map shown in Figure 3.14 [41]. All of these locations have parallel circuits that allow to analyze the power flow regulation capabilities of the HPFC.

Each of the four suggested locations was studied with a hypothetical HPFC installation, and the impact of relevant contingencies (trip of one of the parallel circuits) was investigated. These studies showed that all of these locations are suitable for the installation of the HPFC and would benefit from its addition; however, only the results pertaining to Location d are presented here, since the loading of this circuit is significantly greater (and closer to its limits) compared to the other locations, so that, the impact of the controller can be better examined under normal and contingency conditions. Furthermore, the circuit associated with this location is a crucial link in the grid supplying the main load center of the province, and future demand increases would further stress this interconnection. Therefore, the presented studies for this location are of significant interest and relevance.

Power Flow Results

The double-circuit at Location d connects Trafalgar to Richview, a suburb of Toronto, with each of the parallel circuits carrying roughly 270 MW in the base case. Hence, the HPFC is assumed to be installed on one of the circuits (Line 1), thus controlling its flow directly and the flow of the parallel circuit (Line 2) indirectly. The voltage magnitudes at the controller terminals are assumed to be regulated around a given setpoint, since the controller is considered to start in PVV mode. The basic HPFC parameters used here are the following (100 MVA, 220 kV base):

- Maximum current magnitudes (I_S and I_R): 5 p.u.
- Maximum voltage magnitude for the converters including transformers (V_X and V_Y): 0.05 p.u.
- SVC-based shunt susceptance: $0 \leq B_M \leq 1.5$ p.u.

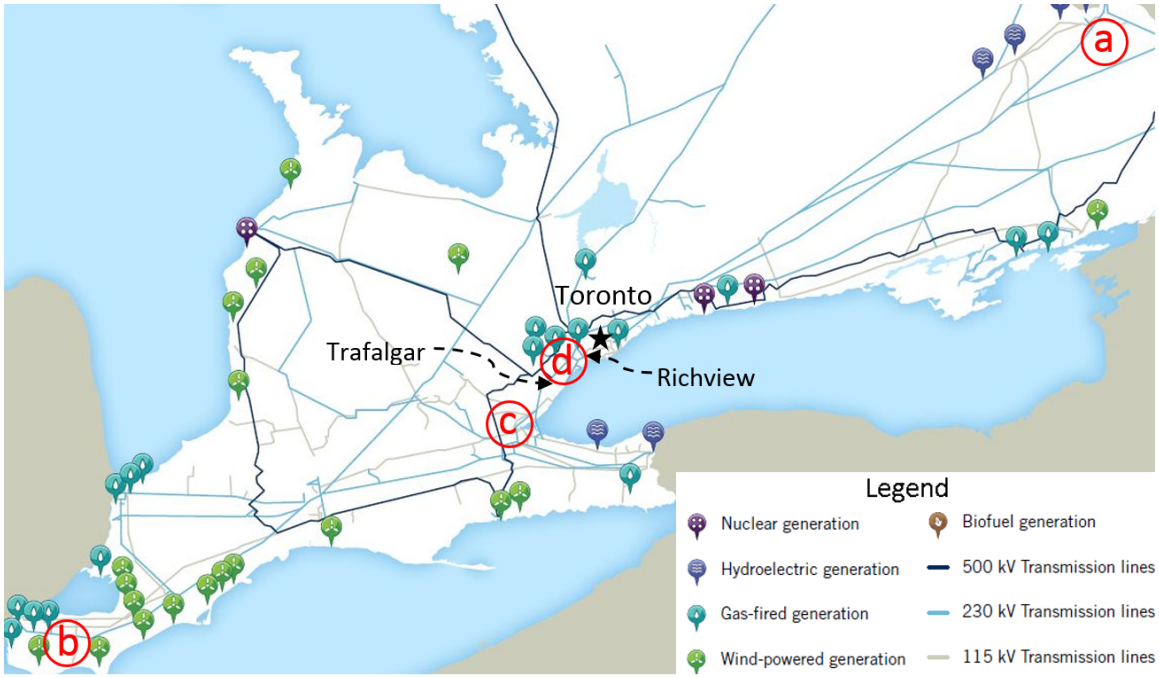

Figure 3.14: Ontario map and potential installation locations of the HPFC [41].

- Range of active-power control in Line 1 with respect to the base case (maximum line rating of 719 MW): 20%–260% (54 MW–700 MW).
- Voltage magnitude setpoint at the terminals (slightly higher than the base-case value of 1.109 p.u.): 1.119 p.u. Note that the voltage magnitudes for the base-case in the Ontario grid correspond to the actual system values provided by the IESO.

To study the impact of the HPFC at the chosen location, the active-power setpoint is gradually increased from 54 MW to 700 MW, while the rest of the system remains intact. Note that this study is different from what was presented in Section 3.2.1, since the load/generation is not altered, with the HPFC regulating flows and voltage magnitudes according to given setpoints. Figure 3.15 shows the active powers flowing through Lines 1 and 2 as the controller setpoints change, until it reaches its capability limits and switches to PQQ mode; this figure highlights the direct and indirect controls over the flows through parallel circuits using the controller.

Figure 3.16 shows B_M and the HPFC control modes highlighting the transition between PVV and PQQ modes. The descending B_M values in PVV mode indicate the increasing need for reactive power at the sending end (Trafalgar) as the active power flow increases. The voltage magnitudes at Trafalgar and Richview remained fixed at their initial values, indicating a stiff system at the lines' terminals.

The change in the active power losses in the Ontario system with the HPFC and different controller setpoints with respect to the base case is illustrated in Figure 3.17. Note that the impact on the system losses is not considerable, due to the stiff nature of the Ontario grid, the sizing of the controller, and the fact that the setpoints chosen for the HPFC approximately match the base-case values.

Figures 3.15 and 3.16 also show the powers, control modes, and B_M values for the controller when Line 2 is tripped, i.e. under contingency conditions. Observe that the controller reaches its limits and changes control modes at lower transfer rates, with the maximum power transfer level saturating at a lower value, as expected.

3.3 Summary

The steady-state model of the HPFC for power flow studies was presented in this chapter, including its multiple control modes and various operating limits. The controller's application to a two-area test system as well as the Ontario-Canada grid addressing congestion

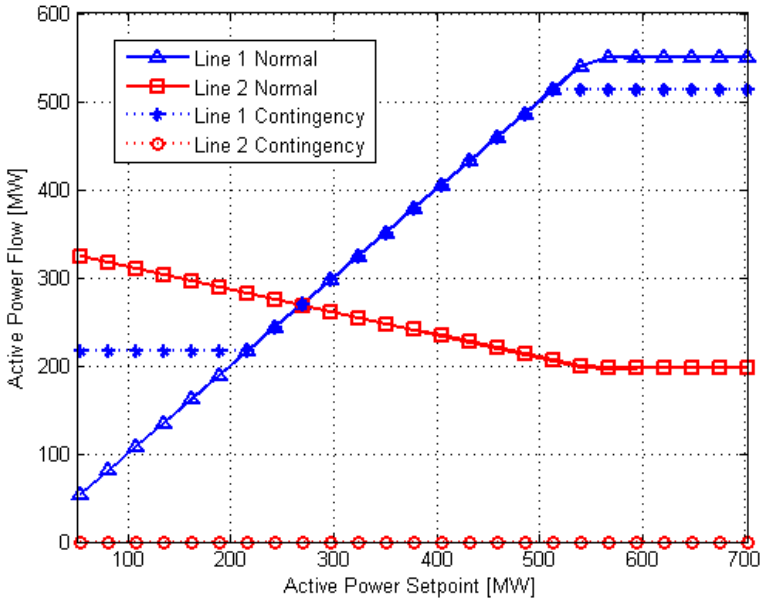

Figure 3.15: Active power flow in the parallel circuits at Ontario's grid Location d.

problems in these networks were discussed in some detail. The presented analyses demonstrated the performance, effectiveness, and feasibility of the controller to solve congestion issues in a real grid.

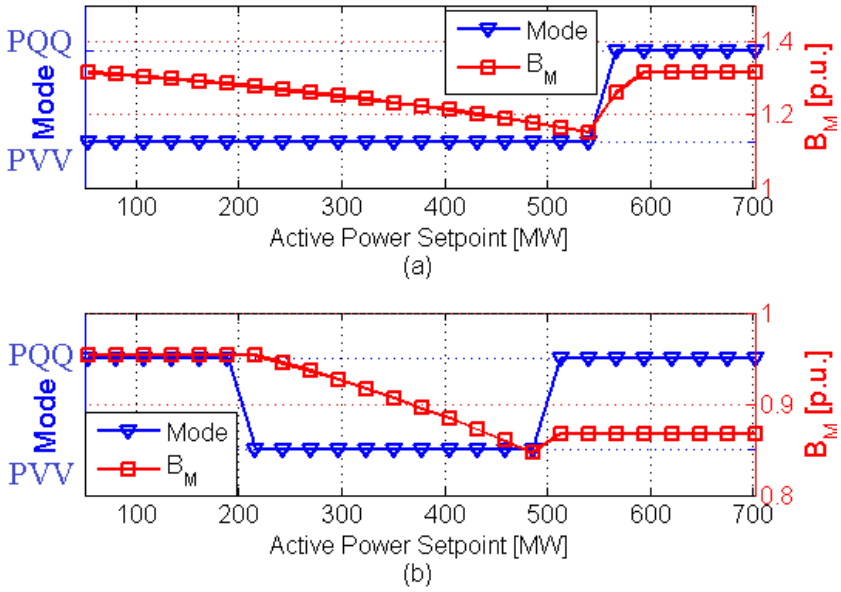

Figure 3.16: HPFC control modes and B_M as the loading level increases for Ontario's grid Location d under: (a) normal, and (b) contingency conditions.

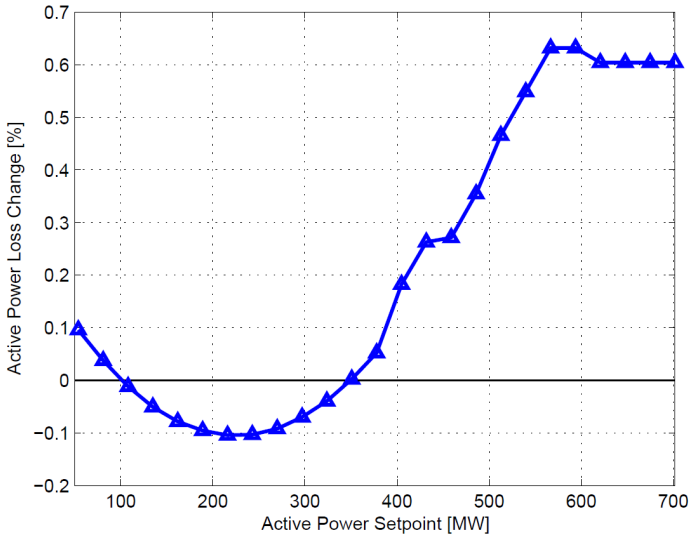

Figure 3.17: Change in active power loss in the system with the HPFC at Ontario's grid Location d with respect to the base case.

Chapter 4

HPFC Optimal Power Flow Modeling

This chapter reports on a detailed model of the HPFC for OPF studies for controller ratings and dispatch purposes. The model is discussed first, properly representing the current and voltage ratings of the device and its components as well as different operating limits of the network. This model is then applied to a benchmark two-area test system using AMPL as the optimization problem solver, with the presented results demonstrating how the HPFC is rated and dispatched within the feasible region, while keeping the controller within its limits and satisfying the desired control objectives.

4.1 Model

The optimal power dispatch for a system can be calculated using an OPF formulation; the objective of this optimization problem is usually the maximization of social welfare or the minimization of production costs. System operational and security constraints as well as operating limits are usually included in an OPF formulation. Hence, mathematically the

OPF can be stated as follows [26]:

$$\min_{P_G, Q_G, V, \delta} \quad Costs = \sum_{k \in \mathcal{G}} C_k \left(P_{Gk} \right) \tag{4.1a}$$

s.t.

$$P_{Gk} - P_{Dk} = \sum_{l \in \mathcal{N}} V_k V_l (G_{kl} \cos(\delta_k - \delta_l) + B_{kl} \sin(\delta_k - \delta_l)) \qquad k \in \mathcal{N} \tag{4.1b}$$

$$Q_{Gk} - Q_{Dk} = \sum_{l \in \mathcal{N}} V_k V_l (G_{kl} \sin(\delta_k - \delta_l) - B_{kl} \cos(\delta_k - \delta_l)) \qquad k \in \mathcal{N} \tag{4.1c}$$

$$P_{Gk\,\min} \leq P_{Gk} \leq P_{Gk\,\max} \qquad k \in \mathcal{G} \tag{4.1d}$$

$$Q_{Gk\,\min} \leq Q_{Gk} \leq Q_{Gk\,\max} \qquad k \in \mathcal{G} \tag{4.1e}$$

$$V_{k\,\min} \leq V_k \leq V_{k\,\max} \qquad k \in \mathcal{N} \tag{4.1f}$$

where $C_k(\cdot)$ stands for the generator i production cost, which is typically a quadratic function; $\mathcal{N}$ and $\mathcal{G}$ represent the set of all buses and generators, respectively; P_D and Q_D stand for the active and reactive demand, which are assumed fixed here; P_G and Q_G represent the active and reactive powers of generators; G_{kl} and B_{kl} stand for line parameters; and V and δ correspond to the bus voltage phasor magnitudes and angles. Line flow limits can also be included in this model; however, for the purpose of the studies presented here, these were not considered, without loosing generality.

A lossless HPFC is considered here as part of the transmission system assets for dispatch purposes. In this context, the device can be represented in the OPF using the following power and circuit equations associated with Figure 3.2:

$$P_{HPFC_1} = Re\left\{ \boldsymbol{V}_{HPFC_1} \boldsymbol{I}_S^* \right\} \tag{4.2}$$

$$P_{HPFC_2} = Re\left\{ \boldsymbol{V}_{HPFC_2} \boldsymbol{I}_R^* \right\} \tag{4.3}$$

$$P_{HPFC_1} = P_{HPFC_2} \tag{4.4}$$

$$\boldsymbol{V}_{HPFC_1} = \boldsymbol{V}_X + \boldsymbol{V}_M \tag{4.5}$$

$$\boldsymbol{V}_{HPFC_2} = \boldsymbol{V}_Y + \boldsymbol{V}_M \tag{4.6}$$

$$\boldsymbol{V}_M = \left(\frac{\boldsymbol{I}_S - \boldsymbol{I}_R}{jB_M} \right) \tag{4.7}$$

Where $_{HPFC}$ subscript refers to the HPFC terminals. Proper ratings of the device imply a symmetrical loading on the series inverters, since both are assumed to share the load equally; this results in the following constraint:

$$|V_X - V_Y| \leq \varepsilon \tag{4.8}$$

where ε is a small tolerance. Furthermore, the ratings of the converters and the shunt capacitor impose limits on the voltage magnitudes V_X and/or V_Y, and current magnitudes I_S and/or I_R, and B_M; these limits can be modeled through the following constraints:

$$0 \leq V_X \leq V_{Xmax} \tag{4.9}$$

$$0 \leq V_Y \leq V_{Ymax} \tag{4.10}$$

$$0 \leq I_S \leq I_{Smax} \tag{4.11}$$

$$0 \leq I_R \leq I_{Rmax} \tag{4.12}$$

$$0 \leq B_M \leq B_{Mmax} \tag{4.13}$$

Adding the HPFC equations and constraints (4.2)–(4.13) to (4.1) yields the full OPF model of the system including the HPFC for dispatch purposes, which was implemented here in AMPL and solved using Knitro solver as discussed in Section 2.6.3. The solution of this optimization problem can be used to determine:

- The power dispatch of the system at minimum cost or maximum social benefit.
- The optimal setpoints of the HPFC control variables, including terminal voltage magnitudes and the device power flows.

In other words, the OPF solution yields an optimal power dispatch and the HPFC optimal control setpoints, corresponding to the lowest system operating costs for the assumed constraints. Also, this formulation, with proper bounds for the HPFC constraints, is used here to determine optimal ratings of the device in design and planning studies for the given system constraints.

4.2 Results

The generators in the area to the right of Figure 4.1, i.e. Buses 3 and 4, which are closer to the demand centre, are assumed to be more expensive than the generators in the left

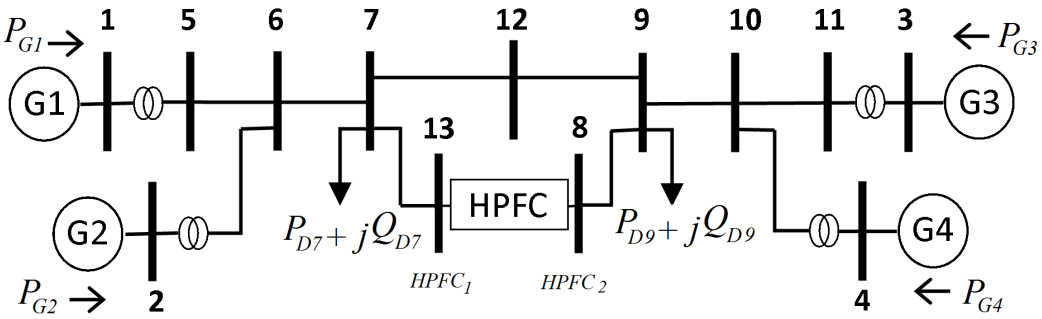

Figure 4.1: Two-area test system for OPF studies.

area (Buses 1 and 2), as per the system data provided in Appendix A. This uneven pricing allows to study the financial impact of the tie-line transfer capability, to be relieved by the introduction of the HPFC.

The ratings of the HPFC can be first obtained using the OPF formulation. Thus, assuming a shunt capacitor, which would represent the HPFC in Z mode, the maximum allowed values for the controller's main variables obtained by solving the OPF are $I_{Smax} = I_{Rmax} = 2$ p.u., and $B_{Mmax} = 0.8$ p.u. (these values were used in the power flow studies in Chapter 3). The voltage ratings of the series converters, however, cannot be obtained this way, since an upper bound is needed due to converter voltage constraints; hence, an upper bound of 0.10 p.u. (23 kV) was assumed for the series-converter voltage ratings, to keep the controller ratings and price reasonably low, and ten different values were considered for V_X and V_Y limits in increments of 0.01 p.u., so that the optimal controller voltage ratings can be determined through multiple OPF solutions, as described next.

The loading level at Bus 9 is gradually increased in 0.3 p.u. steps up to its maximum feasible value of 4.8 p.u. (480 MW), obtained from solving the OPF model; without the HPFC, the maximum value is 4.2 p.u. (420 MW). Note that the maximum loading is different from the one presented in Section 3.2.1, since the OPF problem yields optimal active and reactive power dispatches for the generators, resulting in better overall voltage profiles. The active powers flowing through the lower corridor are shown as the load increases in Figure 4.2 for different series-converter voltage ratings; as expected, higher voltage ratings can accommodate higher power transfers between the two areas.

Observe that as the voltage ratings decrease, the HPFC loses power control at lower demand levels, since the device reaches its current limits sooner, as expected. Note that

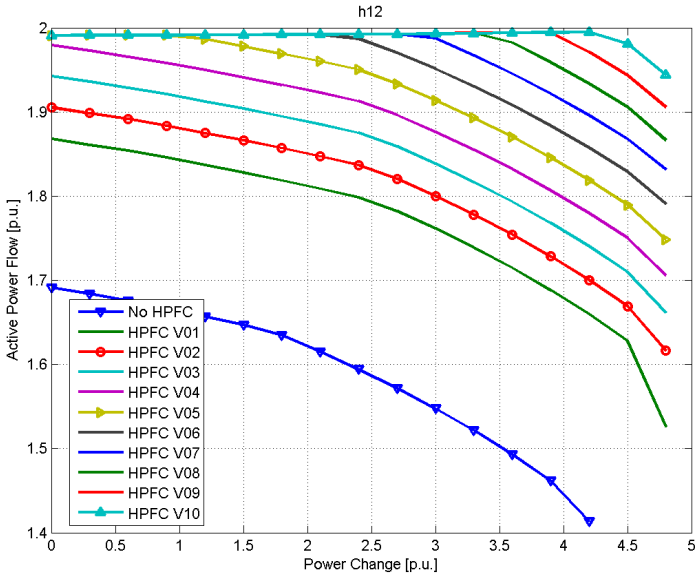

Figure 4.2: Active power flow on the lower corridor of the two-area system for different HPFC voltage ratings.

the OPF analysis directly yields the optimal setpoints associated with the HPFC operating mode (typically PVV mode).

Figure 4.3 compares the difference in average hourly production costs between the systems with and without HPFC for different voltage ratings, which can be regarded as hourly operating savings. From these hourly savings, the expected annual operation savings due to the device installation can be calculated using the typical load duration curve depicted in Figure 4.4 [41], where the maximum and minimum load levels in this curve are mapped to the maximum and minimum load levels chosen from the loadability study, illustrated in Figure 4.2, to cover a year (100% on the time axis of Figure 4.4). Note that a load duration curve provides the percentage of the total time that load is greater or equal to a certain load level; thus, the savings should be the weighted sum of those savings with respect to the percentage of the time that the load is assumed at a certain level as shown for different HPFC voltage ratings in Figure 4.5. The expected annual operation savings due to the device installation are shown in Figure 4.6(a). Observe that the savings increase as the voltage ratings increase, as expected. A cost-benefit analysis is presented next.

The unit cost of converters and their installations depend on several factors; however, in general, a figure of $50,000/MVA can be considered as a reasonable estimate for the

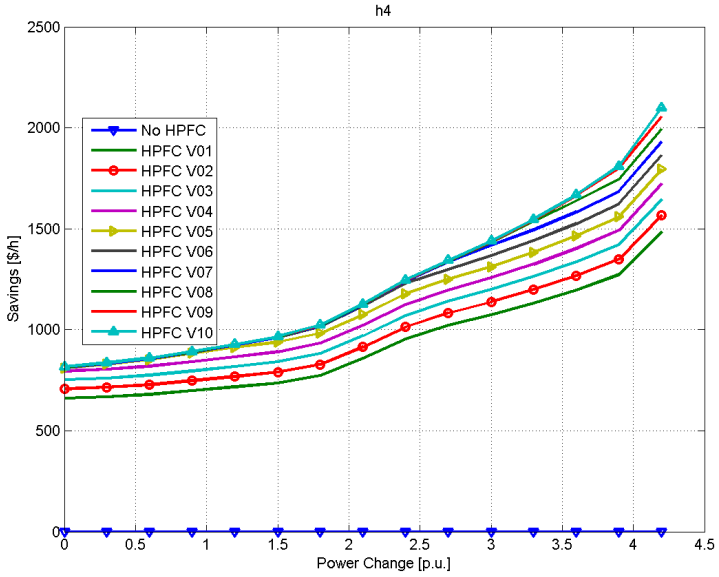

Figure 4.3: Hourly savings in the two-area system compared to the case without HPFC for different HPFC voltage ratings.

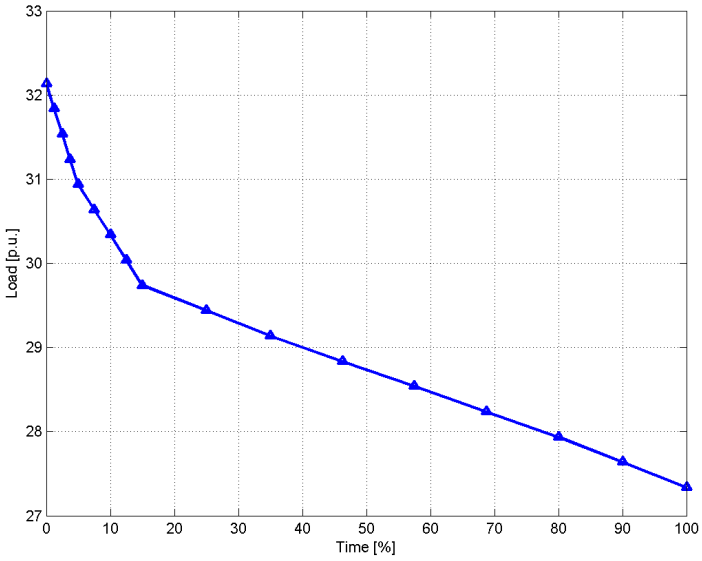

Figure 4.4: Typical annual load duration curve for the two-area test system.

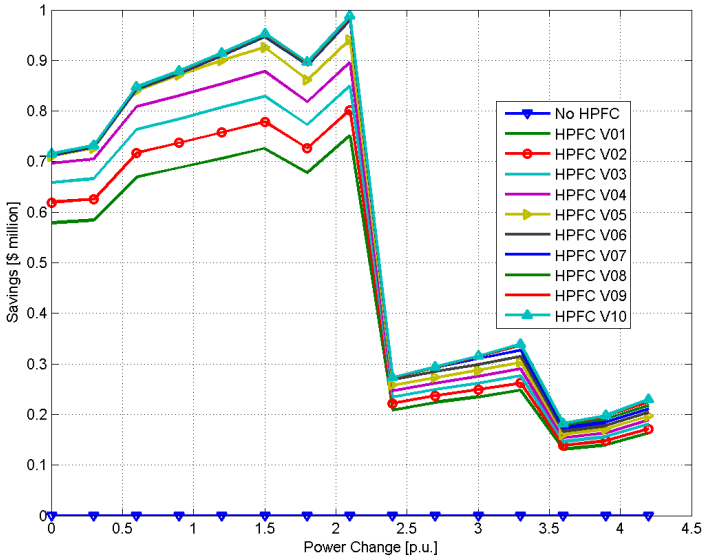

Figure 4.5: Hourly-mapped savings in the two-area system for different HPFC voltage ratings.

Table 4.1: Hardware cost calculations example

			S [p.u.]	S [MVA]	Unit [$ k]	No.	Cost [$ k]
Converter	I_{rated}	2 p.u.	0.12	12	50	2	1,200
	V_{rated}	0.06 p.u.					
Cap. Bank	B_{rated}	0.8 p.u.	0.8	80	10	1	800
Construction							2,000
Total							4,000

hardware cost [42]. For the capacitor banks, this figure is close to $10,000/MVAr. The total installation costs can be roughly approximated as double of the hardware costs, which mainly accounts for the construction costs [43]. For example, the estimated cost for an HPFC installation with voltage ratings of 0.06 p.u. is shown in Table 4.1.

One can compare the effect of different voltage ratings by subtracting the installation costs from the savings in Figure 4.6(a), resulting in the cost-benefit curve depicted in Figure 4.6(b), which has a maximum at a 0.04 p.u. voltage rating. Observe that the estimated benefits for the first year would be already positive in this case, thus justifying the introduction of the HPFC in the test system.

Brief Cost Comparison

Although the main focus of this work is to provide the tools and models to facilitate comparisons between the HPFC and other similar FACTS controllers, this section presents a brief comparative analysis. The figures provided here give a general overview of the performance and impact of the HPFC on the system with respect to other available FACTS options. It should be added that the presented numbers are based on the costs reported in the published literature as well as private communications with industry partners and contacts [44].

Table 4.2 shows approximate cost figures for SVC, STATCOM, UPFC, and HPFC with similar ratings normalized with respect to the cost of the UPFC. Moreover, these controllers offer different benefits and performance characteristics for the system; in other words, they can regulate various variables, and thus, offer different degrees of freedom to the system operator as shown in the table. Observe that the HPFC could provide a similar performance to that of a UPFC with approximately a third of the prospective costs [9].

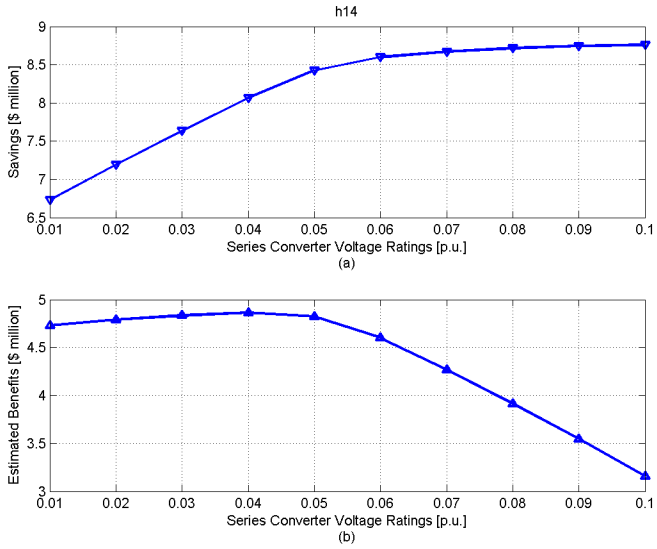

Figure 4.6: Annual economic analysis for different voltage ratings: (a) Savings, and (b) cost-benefit.

4.3 Summary

A detailed model of the HPFC for OPF studies was presented in this chapter. The current and voltage ratings of the device and its components as well as different operating limits of the network were represented properly in the model. The model was applied and studied in a two-area benchmark system, using AMPL with Knitro as the optimization problem solver. The results demonstrated how the controller can be optimally rated and dispatched, within all required operating and HPFC constraints, while minimizing the desired objective

Table 4.2: Comparison of different FACTS controllers

FACTS Controller	Relative Cost	Degrees of Freedom
SVC	40%	1
STATCOM	50%	1
UPFC	100%	3
HPFC with Capacitor Bank	30%	3

function based on realistic pricing parameters.

Chapter 5

HPFC Dynamic Modeling

This chapter models and studies the dynamic behavior of the HPFC and its components and necessary controls under different operating conditions. Considering the various and prominent challenges faced by electric power distribution systems in the context of smart grids, and the capital-intensive nature of a FACTS installations at the transmission level, in this chapter, the focus is on the application of the HPFC to distribution system. The controller is modeled and implemented in PSCAD/EMTDC, with all its control strategies and associated systems, using a distribution test system based on the North American CIGRE distribution benchmark network. The results illustrate the effective performance of the controller for the improvement of voltage sags triggered by fault conditions, and regulation of power fluctuations due to renewable energy resources.

5.1 HPFC Modeling and Control

The operation of the HPFC within limits, in PVV or PQQ mode, yields three degrees of freedom available for deployment as discussed in detail in Chapter 3; this is the basis of modeling in this chapter. The detailed modeling and control scheme of the controller are discussed in this section, considering that the dynamic control of the HPFC directly regulates system currents. Thus, based on the power flow setpoints and other system variables, current reference points are obtained and fed into the main control loop to achieve the desired output. Furthermore, a master-slave control scheme is proposed here to regulate the shunt voltage magnitude while controlling the output power flow variables, since regulating the shunt voltage is necessary to keep the ratings of the converters low and thus make the controller more affordable.

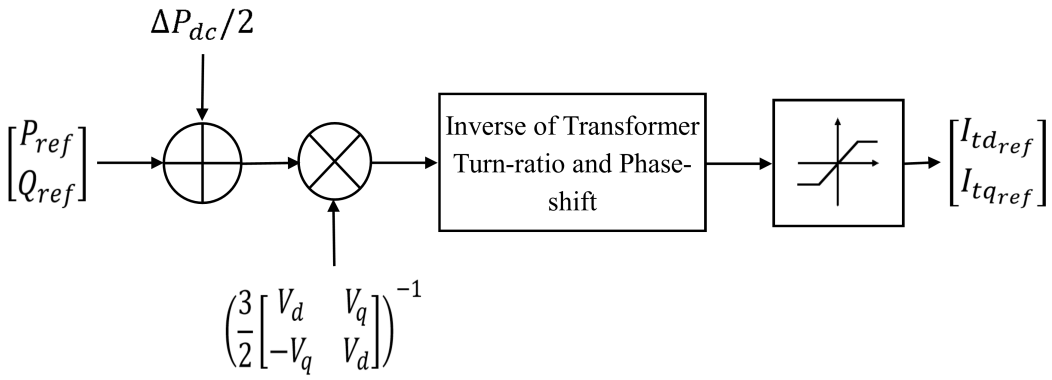

Figure 5.1: Current reference based on power setpoint.

The HPFC converters exchange active power through the dc link, with the flow through the link and losses in the controller components affecting the dc voltage level; thus, proper operation of the controller requires dc voltage regulation, which can be achieved via a separate control loop. Finally, a control procedure is required to start up the HPFC. All these different controls are described in detail next.

5.1.1 Current Control

The current reference is obtained based on the system measurements and power flow setpoints provided by the operator, as discussed in Chapter 4. In Figure 5.1, assuming that active and reactive power output at the HPFC terminal (e.g. Terminal 2) is given as the setpoint in PQQ mode, the dq components of the current reference are obtained. The effect of the transformer turn-ratio as well as its phase shift, based on the connection type, should be included in the calculations. Limiter blocks at the output remove any unreasonably large values or spikes. An auxiliary signal $\Delta P_{dc}/2$ can be added to the active power reference point to account for internal losses and the dc-link voltage regulation, as explained in Section 5.1.4.

The closed loop control of current is realized using proportional-integral (PI) controllers in the dq-reference frame. The output of the current control loop provides a voltage setpoint which is compared with a modulating triangular signal to create switch firing signals based on a PWM scheme.

In Figure 2.3 depicting the VSC filter, if the switching frequency w_s is significantly larger than R/L and the filter parameters are chosen properly, then the high-frequency components of the input does not contribute significantly to the output and the ripple would be small. Under this assumption, the relationship between the in/out voltage and current in the dq-reference frame of the VSC can be written as follows, based on Figure 2.2:

$$V_{gd} = V_{td} + wLI_{tq} + RI_{td} - w^2LCV_{td} + RCwV_{tq} \tag{5.1}$$

$$V_{gq} = V_{tq} - wLI_{td} + RI_{tq} - w^2LCV_{tq} - RCwV_{td} \tag{5.2}$$

These equations can be considered as an open-loop system with the currents $I_{t_{dq}} = [I_{td}\ I_{tq}]^T$ as the output and voltages $V_{g_{dq}} = [V_{gd}\ V_{gq}]^T$ as the input, with the control objective being the regulation of $I_{t_{dq}}$. This can be achieved via the closed loop system shown in Figure 5.2, in which the reference command is compared with the measured value, and the error signal is passed through a PI controller to generate the desired output. The outputs of the PI controller and the control loop must be limited properly.

The parameters K_p and K_i of the PI controllers can be chosen to cancel the pole created due to the presence of the filter L at the output of the converter. Therefore, the equivalent control path from the current reference to the output value becomes a first-order lag with a time constant τ. Thus, based on the values of the circuit elements R and L, and the design parameter τ:

$$K_p = \frac{L}{\tau} \qquad\qquad K_i = \frac{R}{\tau} \tag{5.3}$$

It is important to note that the time constant τ should be small to provide a fast current-control response; however, this should be large enough so that $1/\tau$ is considerably smaller than the switching frequency w_s [31]. The upper constraint is required to be able to neglect high order harmonics, so that the output follows the fundamental-frequency component of the reference signal.

5.1.2 Terminal Voltage Control

In the previous section, it was assumed that reference values were provided for active and reactive power flows at the device terminals for the HPFC in PQQ mode, as per Figure 5.1. However, for distribution system applications, it is better to control the voltage magnitude at a given controller terminal rather than controlling the reactive power supplied/absorbed, due to the importance of maintaining adequate voltage profiles in distribution networks, so that the HPFC normally operates in PVV mode. Therefore, a control loop for regulating

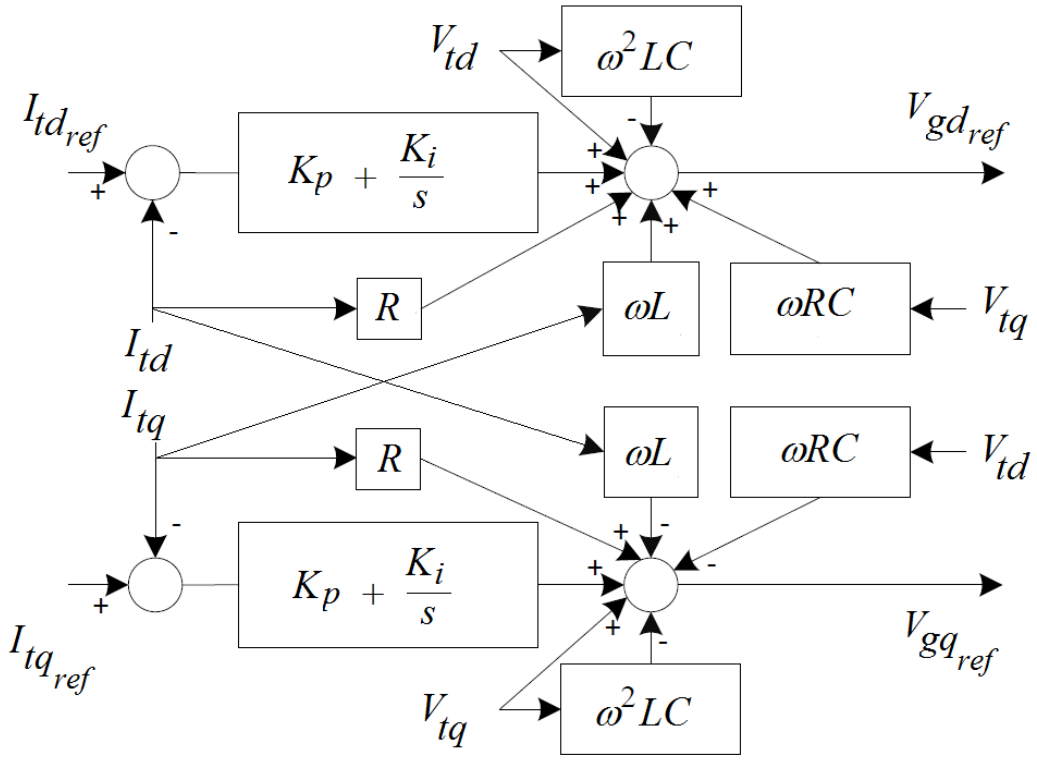

Figure 5.2: Current control loop.

the voltage magnitude at the device terminal (e.g. Terminal 2 in Figure 3.2) is required, as shown in Figure 5.3, where the reference voltage for V_2 is compared with the measured value, and the error signal is passed through a PI controller to generate the required reactive power reference in Figure 5.1.

The described control approach requires a nested (hierarchical) control structure; therefore, the closed loop bandwidth of the outer loop (voltage control) should be adequately lower than the inner current control loop. In other words, the PI-controller parameters are chosen so that the time constant of the voltage control loop is considerably larger than the current-control loop time constant τ.

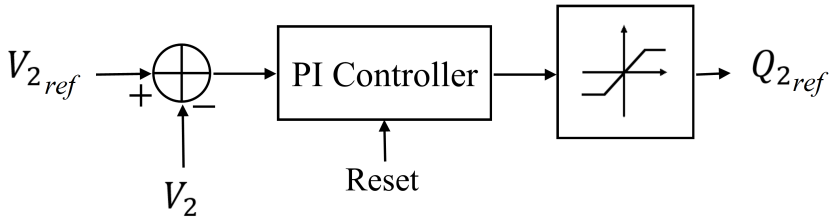

Figure 5.3: Terminal 2 voltage control loop.

5.1.3 Shunt Voltage Control

The voltage magnitude on the inverters output depends on the shunt device voltage. It is desirable to keep the ratings of the converters low and thus affordable; therefore, it is important to be able to control the shunt voltage within an acceptable range while achieving the desired power flow setpoints. As stated previously, the HPFC can control three independent variables among the terminal variables (e.g. P_2, Q_1, and V_2 in Figure 3.2); hence, one of these degrees of freedom can be used to regulate the shunt voltage V_M instead of a reactive power (e.g. Q_1).

The closed-loop control of the shunt voltage can be accomplished as follows: The control scheme for one of the converters (e.g. Converter 2) is preserved, as explained in the previous sections; namely the terminal active power and voltage magnitude are regulated at the controller terminal. Hence, the reference values used in the control loops of the other converter (e.g. Converter 1) can be obtained based on the desired active power flow and shunt voltage magnitude as well as the measured currents at the other terminal (e.g. Terminal 2). Referring to the parameters and variables defined in Figure 3.2, this control scheme can be realized using the following set of equations:

$$2V_M^2 B_M^2 = (I_{Sd} - I_{Rd})^2 + (I_{Sq} - I_{Rq})^2 \tag{5.4a}$$

$$P_1 = P_{ref} \tag{5.4b}$$

$$V_M = V_{Mref} \tag{5.4c}$$

This set of equations after simplification results in equations in the dq domain, which have two sets of solutions for the current setpoint associated with two Q_1 reference values, which in turn are associated with two $V_{M_{dq}} = [V_{Md}\, V_{Mq}]^T$ values equal in magnitude and 180° out of phase; a solution can be chosen based on the design requirements or operator preferences. Similarly to Figure 5.1, the current reference should be limited and corrected for the transformer ratio and connection type before being used in the current control loop shown in Figure 5.2.

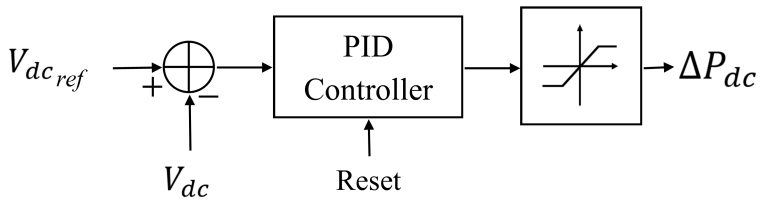

Figure 5.4: DC voltage control loop during steady state.

5.1.4 DC Regulation

The dc-capacitor connecting the two converters provides a path to exchange power between them, while regulating the power flows at the HPFC terminals. However, the voltage level across this capacitor has a direct impact on the converters' performance. The controller losses and any net power flowing in/out of this capacitor would change its voltage and thus, might compromise the performance of the controller. Therefore, it is important to monitor and control the dc-voltage level V_{dc} by compensating for losses and the charging and discharging of the dc capacitor through the converters.

A PID (proportional-integral-derivative) controller is used here to regulate the dc-link voltage, since its steady-state error is zero and the transient performance is well-damped due to the derivative block, as the feedback from the dc-capacitor current is proportional to the derivative of the capacitor voltage. This is accomplished by changing the active power setpoints of the converters by the $\Delta P_{dc}/2$ shown in Figure 5.4. In other words, using the auxiliary signal in Figure 5.1, ΔP_{dc} is shared equally between the converters to minimize the deviations from the original setpoints.

5.1.5 Start-up Control

It has been so far assumed that the dc-link is charged and initialized prior to the device utilization. Although one could use an external converter or energy storage device to initially charge the HPFC dc capacitor, a cold start-up is possible using the initialization procedure explained next.

The proposed charging procedure starts by using the anti-parallel diodes of one of the converters as a 3-phase diode rectifier bridge to charge the capacitor to a certain voltage level in an uncontrolled way. Then, the switches are appropriately controlled to charge the dc capacitor up to a desired voltage level. The control does not need to be precise,

Table 5.1: DC-link start-up procedure

Stage	Activity
I	Uncontrolled charging using diode rectifiers.
II	Charging to a given level through switch control.
III	DC-link control deactivated (buffer zone).
IV	DC-voltage regulation in normal operation using PID controller (Section 5.1.4).

since it only serves to initialize the dc link. There is a buffer zone in which there is no dc-link control before the normal dc-regulator loop is activated, thus allowing V_{dc} to reach its steady-state value. Therefore, there are four stages in the proposed start-up procedure as shown in Table 5.1. The results presented in the next section show that this strategy is quick, as it reaches steady state in seconds; flexible, as it can be tailored to any system; and economic, since no auxiliary systems are required.

In Table 5.1, Stages I and III are straightforward, and Stage IV was discussed in Section 5.1.4. Regarding Stage II, it is preferable to charge dc capacitors with a constant current instead of a constant voltage [45]. Note that the main control loop (Figure 5.1) accepts power setpoints; therefore, it is necessary to translate a constant current to a power input during the dc charging in Stage II. Hence, the balance of power based on average values ignoring losses yields:

$$P_{in} = V_{dc} I_{dc} \tag{5.5}$$

where I_{dc} is the dc-link current, and P_{in} is the charging power flowing into the converter and absorbed by the dc-link. Assuming a constant charging current, one has:

$$V_{dc} = \frac{1}{C_{dc}} \int_0^t I_{dc} dt \quad \Rightarrow \quad V_{dc}(t) = \frac{I_{dc}}{C_{dc}} t + V_{dc0} \tag{5.6}$$

where V_{dc0} is the initial dc voltage achieved using anti-parallel diodes in Stage I. Substituting (5.6) in (5.5):

$$\begin{aligned} P_{in}(t) &= \frac{(I_{dc})^2}{C_{dc}} t + V_{dc0} I_{dc} \\ &= \alpha t + \beta \quad \alpha, \beta > 0 \end{aligned} \tag{5.7}$$

This power is given as an input to the power control loop in Figure 5.1, so that $P_{ref} = -P_{in}(t)$, with $Q_{ref} = 0$; in other words, the reference power would linearly decrease. Note that (5.7) is an approximate formulation based on average values and does not result in an ideally fixed charging current; regardless, the proposed charging procedure is effective and simple to implement.

5.2 Results

The HPFC can improve a distribution system in two main and distinctive ways, namely, it can supply/absorb reactive power and improve voltage profiles, and it can also regulate active power flow in a specific corridor. Therefore, in this section, the HPFC performance is studied in a distribution system under fault conditions, which lead to sudden voltage changes, and in the presence of intermittent energy resources, which cause active power fluctuations [46].

5.2.1 Test System

The performance of the controller under different operating conditions is demonstrated using a 12.7 kV test system based on the CIGRE benchmark for medium voltage distribution networks [47]. The system and the controller at the switch level are implemented in PSCAD/EMTDC using standard library components [15]. The general schematic of the test system is shown in Figure 5.5, with its data provided in Appendix C; the total load is assumed to be balanced, distributed among the buses connected via feeders modeled as coupled-pi sections.

Switches S1 and S2 are assumed to be open; thus, there is no connection between Buses 8-14 and 6-7. Switch S4 can connect a solar photovoltaic generator (SPVG) to Bus 5, as discussed in Section 5.2.4 [48]. Switch S3 has three possible positions, namely, open (O), closed (C), and closed through an HPFC (H), thus, creating three different system configurations; these study scenarios are referred here to as O, C, and H, respectively. The values of the main parameters of the HPFC are shown in Table 5.2.

5.2.2 DC Start-up and Regulation

The dc link of the converters needs to be initialized during the HPFC start-up and be properly regulated, as presented and discussed in this section. Thus, as mentioned in

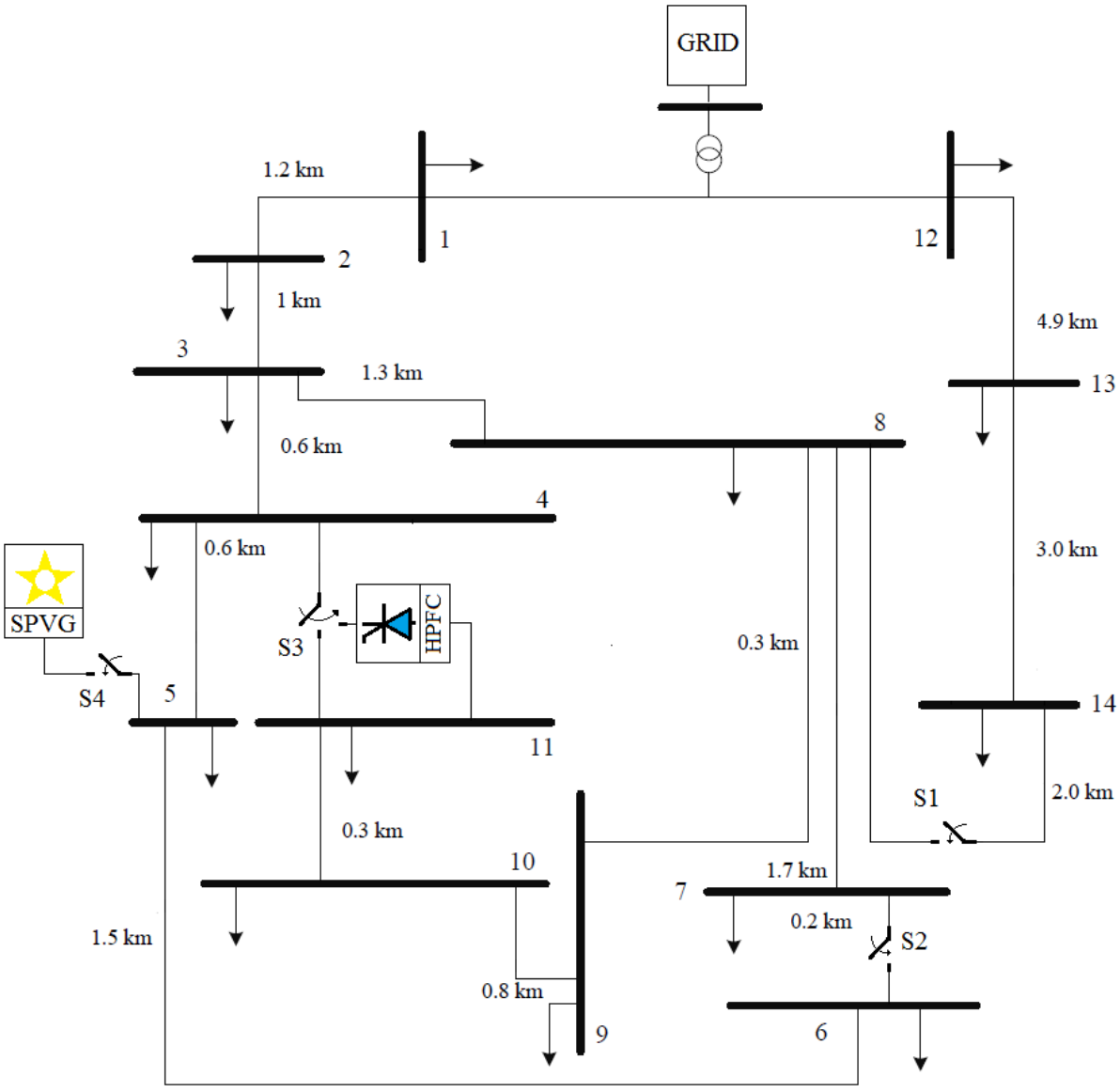

Figure 5.5: Single line diagram of the distribution test system.

Table 5.2: HPFC parameters

Parameter	Value
S_{rated}	4 MVA
V_{rated}	12.7 kV
I_{rated}	180 A
L	68.75 μH
C	39.45 μF
R	10.4 mΩ
f_s	3060 kHz
B_M	0.0754 S
τ	0.5 ms
k_p	6.85
k_i	1040 s^{-1}

Section 5.1.5, the anti-parallel diodes of one of the converters charge the dc capacitor to a certain voltage to start up the controller. The dc link voltage is shown in Figure 5.6a with different sections depicting the various stages of the proposed start-up procedure, and Figure 5.6b illustrates the dynamics of the average current in the dc capacitor.

In Figure 5.6a, observe that the dc-link is initially charged to 1.7 kV, which is the peak-to-peak line voltage available on the primary side of the transformer, using the diodes of Converter 2 in Stage I. Note that the voltage curve resembles that of a charging capacitor through an RC circuit, saturating at some point. With the available initial voltage V_{dc0}, Converter 2 can then control the capacitor charging (Stage II). Thus, assuming $I_{dc} \simeq 1$ kA and a maximum $V_{dc} = 2.7$ kV, α and β in (5.7) can be obtained, and a linearly decreasing P_{ref} can be set in Figure 5.1. The dc-capacitor current during this process is highlighted in Figure 5.6b; observe the initial bump in the current around $t = 0.5$ s due to the controller's shunt ac capacitor, since Converter 1 is off and thus Converter 2 provides a current path for the shunt capacitor through the secondary side of the transformer. Note that the charging current peak should be considered during the converter design phase and for the choice of switches, so that the momentary charging current does not significantly exceed the rated current of the VSC switches.

In Stage III, the dc-control is deactivated and V_{dc} is allowed to drop to its steady-state value of 2.5 kV, as shown in Figure 5.6a; this stage creates a buffer zone between the start-up procedure and the normal operation of the HPFC. Finally, in Stage IV, Converter 1 is connected and normal operation of the controller with regulation of V_{dc} starts roughly at $t = 0.75$ s, when the dc voltage reaches its nominal value.

5.2.3 Fault Conditions

During faults in distribution systems, voltage sags appear in feeders, which can be mitigated using FACTS [49], as presented here for the HPFC. A voltage sag is defined as a voltage drop below a threshold of typically 90% of a declared value, with a duration longer than half a cycle and less than a minute [50]. This can be characterized using the following voltage sag energy index, which can be expressed in cycles, milliseconds, or seconds [50]:

$$E_{VS} = \int_0^T \left[1 - \left(\frac{V(t)}{V_{nom}}\right)^2\right] dt \tag{5.8}$$

where T is the duration of the event, $V(t)$ is the voltage at the point of interest, and V_{nom} is its nominal value. The voltage sag energy index E_{VS} is related to the energy that has not been delivered during the sag. For repetitive sags, which are common in distribution systems, an approach based on standard ride-through capability curves can be used [51].

A three-phase fault at Bus 6 is applied at $t = 2$ s, and is cleared after 50 ms; this fault can be due to a tree branch that causes a brief resistive short circuit, as frequently occurs in distribution systems with overhead feeders. The voltages at Buses 5 and 11 are shown for the three O, C, and H scenarios in Figure 5.7; observe that the voltage profiles improve with the HPFC. The voltage sag energy index is calculated and added for all the load buses for the three system configurations, and the results are shown in Table 5.3, indicating a considerable reduction in E_{VS} with the HPFC. Note that there is no significant difference between the results for cases O and C.

5.2.4 Intermittent Resources

The reports and analyses of the recent solar eclipse in North America recommend better flow control and power regulation capabilities in the system to improve the system response to predictable and unpredictable fluctuations in the variable output of renewable energy resources [52], which can be accomplished with the HPFC, given its effectiveness to regulate

Table 5.3: Voltage sag energy index for cases O, C, and H

Case	E_{VS} [ms]
O	52.2
C	52.2
H	25.1

power flows. To demonstrate this, an SPVG with variable power output is connected to Bus 5 [48]; at full capacity, the unit can equivalently generate 2.8 MW at unity power factor.

The SPVG is modeled using balanced 3-phase current sources in phase with the voltage phase angle measured at the point of connection, to represent pure active power injection associated with an SPVG in PQ mode. To accommodate this extra power generation the system loading is increased at Bus 8 by 1 MW. As depicted in Figure 5.8, in this study, the SPVG unit is initially at steady state, operating at full capacity; at $t = 3$ s, the SPVG output suddenly drops to zero to represent sudden and significant cloud coverage; and at $t = 4$ s, the SPVG gradually ramps up to its initial full level by $t = 4.5$ s.

The three S3 configurations, i.e. O, C, and H, result in the active power flows between buses 4 and 11, normalized with respect to pre-event values, illustrated in Figure 5.8; for O where S3 is open, the flow is zero. Case C shows the response of the system to the change in the power injection at Bus 5. Finally, with the HPFC in the system in Case H, the active power flow remains regulated at the pre-event value as desired. Figure 5.9 depict the current magnitudes at the HPFC terminals to better examine the response of the controller in this case. Note that the dq components of the currents follow the pertaining references with a delay of approximately 4τ.

5.3 Summary

In this chapter, a detailed dynamic model of the HPFC and its controls were proposed, developed, and implemented in PSCAD/EMTDC, including a simple and effective start-up procedure for the controller. The model was used to examine the impact of the device on a benchmark distribution test system under two different conditions, namely, a fault causing a momentary voltage sag, and power flow fluctuations due to a solar photovoltaic

generator. The results showed the capability of the controller to improve a distribution system's response using time-domain simulations.

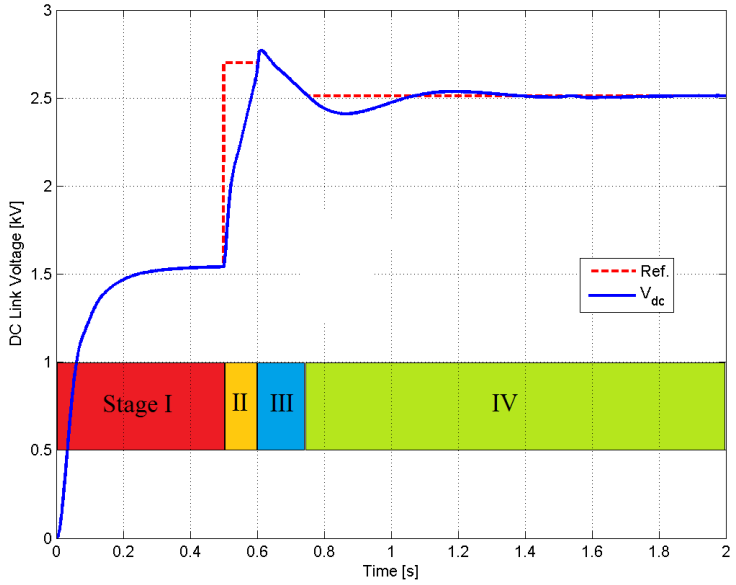

(a)

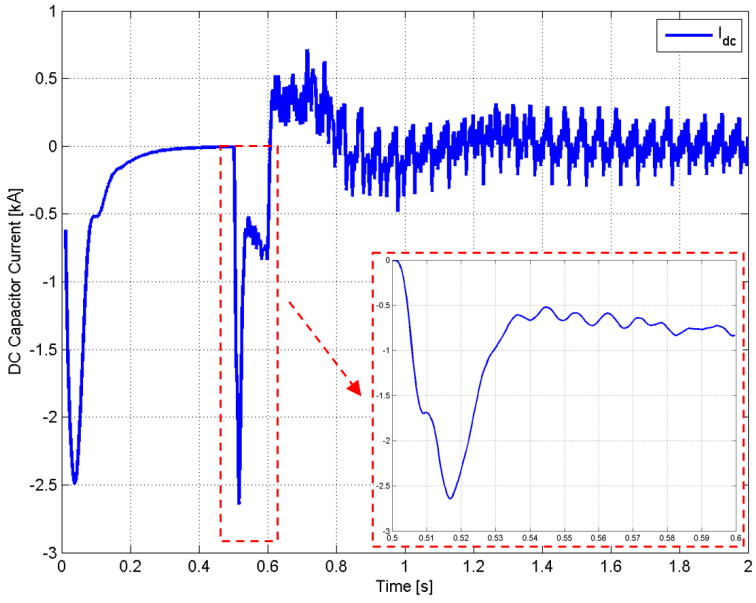

(b)

Figure 5.6: (a) DC-link voltage and (b) average current during start-up stages (Table 5.1).

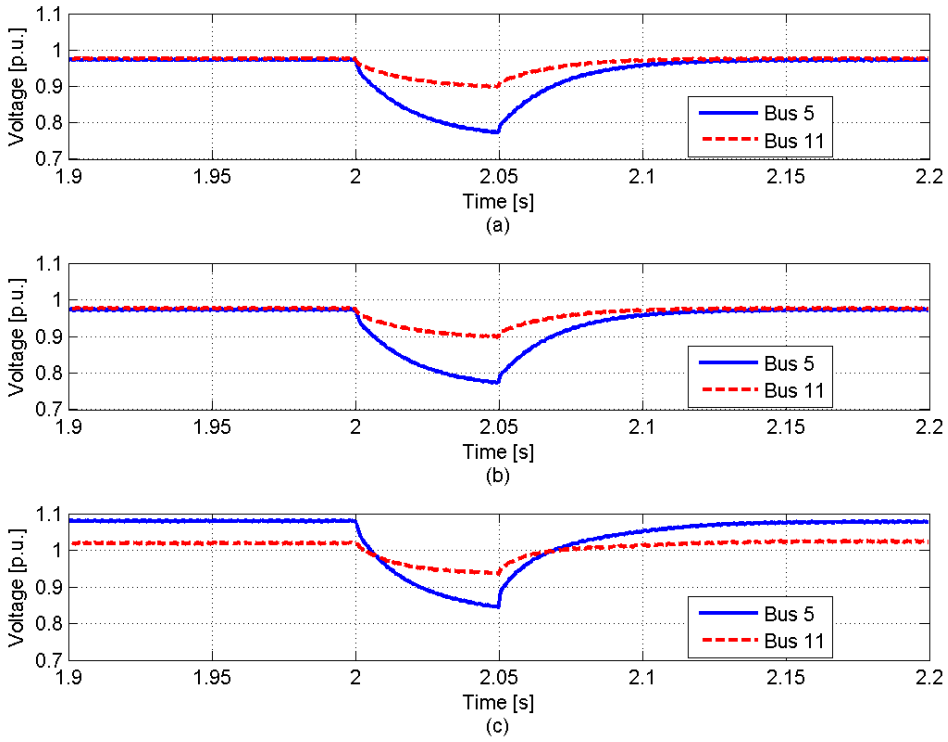

Figure 5.7: Bus voltage magnitudes during a fault for (a) O, (b) C, and (c) H cases.

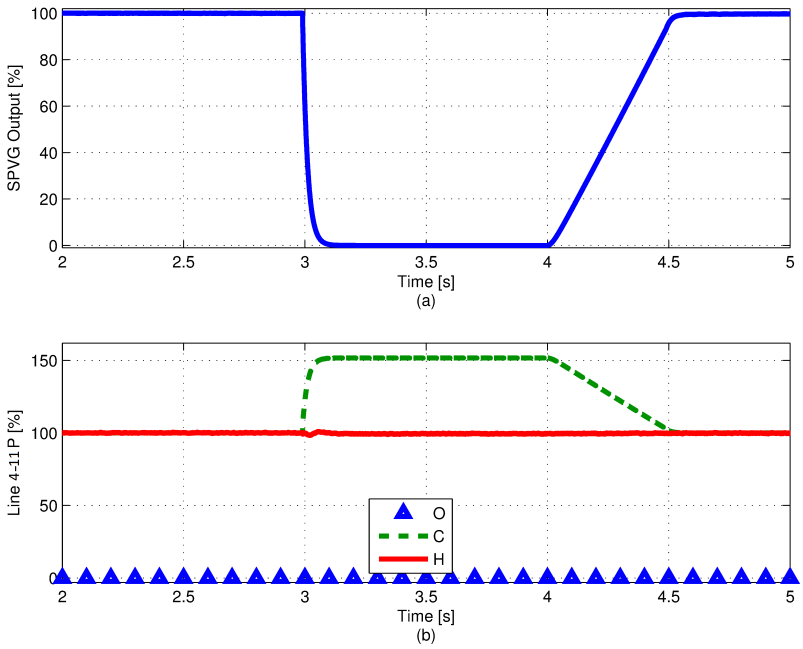

Figure 5.8: Impact of solar power change on Line 4-11 flow: a) SPVG output, b) system response for cases O, C, and H.

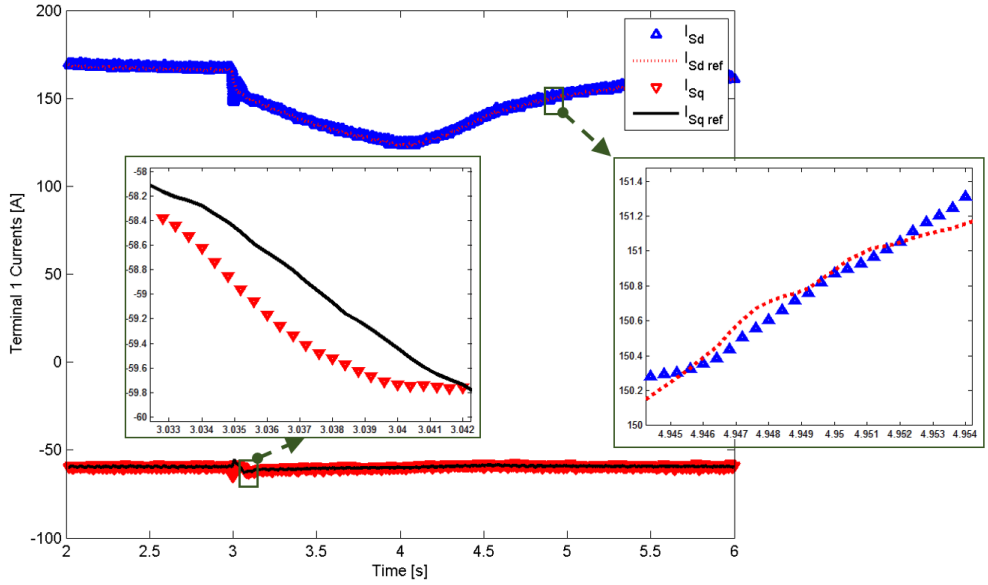

(a)

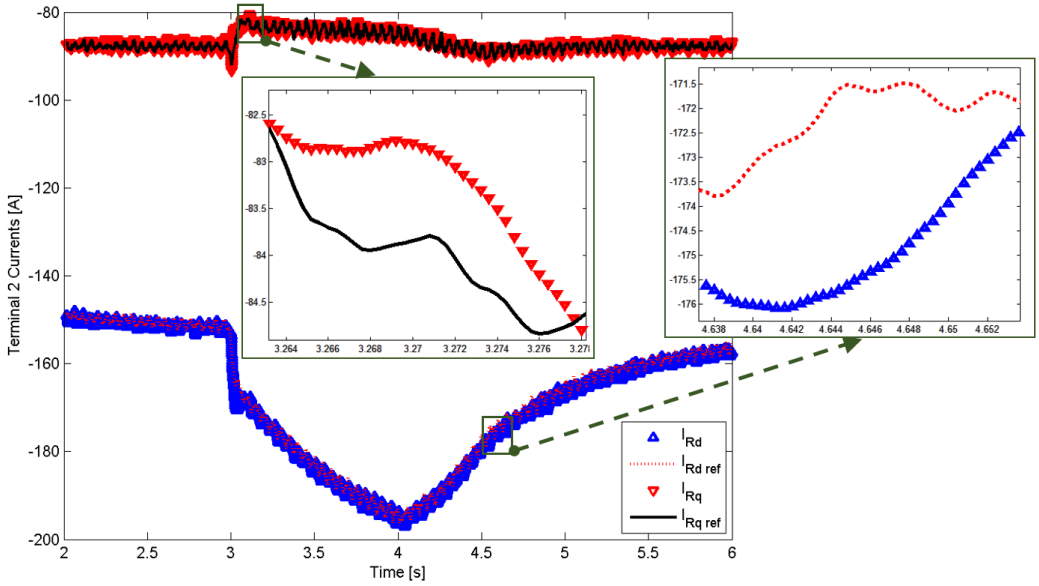

(b)

Figure 5.9: Current magnitudes at (a) Terminal 1 and (b) Terminal 2 of the HPFC.

Chapter 6

Conclusion

6.1 Summary and Conclusions

This thesis studied and proposed power flow, optimal power flow (OPF), and detailed dynamic models of the HPFC, which is a cost effective FACTS controller effective in regulating power system variables at different voltage levels. This controller which consists of converters as well as passive components such as capacitor banks is more economical compared to other similar FACTS controllers, while providing similar regulation capabilities.

Relevant concepts, methods, and tools required for this research work were reviewed in Chapter 2. First, a general overview of the modeling approach used in this thesis and its different stages based on the intended application and target software package were presented. Next, the basics of steady-state power system analyses were discussed, namely, power flow and OPF; the integration of FACTS controllers into these analysis techniques was also discussed, highlighting some related computational implications. Then, a simple architecture of the VSC with its main components, i.e. switches, filter, and typical control approaches, were reviewed before providing a general overview of the HPFC. Finally, several relevant software packages used in the presented research work were also briefly described.

The steady-state model of the HPFC for power flow studies was presented in Chapter 3, including its multiple control modes and various operating limits. The controller's application to a two-area test system as well as the Ontario-Canada grid addressing congestion problems in these networks were discussed in some detail. The presented analyses demonstrated the performance, effectiveness, and feasibility of the controller to solve congestion issues in a real grid.

A detailed model of the HPFC for OPF studies was presented in Chapter 4. The current and voltage ratings of the device and its components as well as different operating limits of the network were represented properly in the model. The model was applied and studied in a two-area benchmark system, using AMPL with Knitro as the optimization problem solver. The results demonstrated how the controller can be optimally rated and dispatched, within all required operating and HPFC constraints, while minimizing the desired objective function based on realistic pricing parameters.

In Chapter 5, a detailed dynamic model of the HPFC and its controls were proposed, developed, and implemented in PSCAD/EMTDC, including a simple and effective start-up procedure for the controller. The model was used to examine the impact of the device on a benchmark distribution test system under two different conditions, namely, a fault causing a momentary voltage sag, and power flow fluctuations due to a solar photovoltaic generator. The results showed the capability of the controller to improve a distribution system's response using time-domain simulations.

In conclusion, the proposed power flow model to represent the device and its operating limits for power flow analysis, which is one of the most widely used and important tools for power system studies, would be useful for the analysis of HPFC applications in practical grids. The presented OPF model could be used in operation and planning studies to optimize grid and HPFC variables, while respecting the capability limits of the controller and other components of the system. Finally, the proposed HPFC model and controls appropriate for time-domain studies and applications would allow evaluating and utilizing the controller in dynamic system functions, especially in distribution systems. Therefore, the outcome of this research work provides essential models and controls to comprehensively study and apply HPFC in practical power systems at different voltage levels and purposes.

6.2 Contributions

The main outcome and contributions of this research work are the following:

- Models and Controls: Developed concise, proper, and practical mathematical formulations and controls of the HPFC for different practical applications and time frames, i.e. steady-state and electromagnetic transients, considering the capability limits of the device operation and its various controls.
- Software Implementation: Implemented the proposed models in research and commercial software packages used for power flow, OPF, and time-domain analyses, in particular, AMPL, PSAT, PSS®E, and PSCAD™/EMTDC™.

- Practical Studies and Applications: Demonstrated the use and applications of the proposed models and controls for practical systems and studies, especially for distribution systems and Ontario's grid, to evaluate the practical impact of the HPFC on these system, including potential benefits from its possible adoption by grid operators.

The results of this work have been published in [53], [54], [55], and [56].

6.3 Future Work

- The shunt component of the HPFC is mainly assumed to be a capacitor bank in this thesis due to its economic advantages. However, other forms of shunt compensation could be also included and studied.
- The developed dynamic models could be exported and integrated into a power system simulator suitable for transient studies, such as PSS®E, which would enable performing stability studies of particular systems such as the Ontario-Canada power grid.
- The models developed and presented in this work could be used to perform comparative studies of the HPFC performance vis-a-vis other relevant controllers, to better evaluate its benefits and shortcomings.

References

[1] X. P. Zhang, C. Rehtanz, and B. Pal, *Flexible ac Transmission Systems, Modelling and Control*. Berlin, Germany: Springer 2006.

[2] J. M. Bloemink and T. C. Green, "Benefits of distribution-level power electronics for supporting distributed generation growth," *IEEE Trans. Power Del.*, vol. 28, no. 2, pp. 911–919, Apr. 2013.

[3] D. Divan and H. Johal, "Distributed FACTS—A new concept for realizing grid power flow control," *IEEE Trans. Power Electron.*, vol. 22, no. 6, pp. 2253–2260, Nov. 2007.

[4] I. Axente, R. K. Varma, and W. Litzenberger, "Bibliography of FACTS: 2000 – part I IEEE working group report," in *Proc. IEEE PES General Meeting*, pp. 1–6, 2011.

[5] N. G. Hingorani and L. Gyugyi, *Understanding FACTS- Concepts and Technology of Flexible ac Transmission Systems*. Delhi, India: Wiley, 2000.

[6] Y. H. Song and A. T. Johns, *Flexible ac Transmission Systems (FACTS)*. London, UK: IEE, 1999.

[7] S. A. Nabavi-Niaki and M. R. Iravani, "Steady-state and dynamic modelling of Unified Power Flow Controller (UPFC) for power system studies," *IEEE Trans. Power Syst.*, vol. 11, no. 4, pp. 1937–1943, Nov. 1996.

[8] S. J. A. Vaseai and S. A. Nabavi-Niaki, "Effect of UPFC converters constraints on loadability characteristic," in *Proc. Transmission and Distribution Conference and Exhibition: Asia and Pacific, IEEE/PES*, pp. 1–4, 2005.

[9] J. Z. Bebic, P. W. Lehn, and M. R. Iravani, "The Hybrid Power Flow Controller - a new concept for flexible ac transmission," in *Proc. IEEE PES General Meeting*, Montreal, Quebec, Canada, pp. 1–8, 2006.

[10] V. K. Sood and S. D. Sivadas, "Simulation of Hybrid Power Flow Controller," in *Proc. Int. Conf. Power Electronics, Drives and Energy Systems (PEDES) & Power India*, pp. 1–5, Dec. 2010.

[11] N. R. Merritt and D. Chatterjee, "Performance improvement of power systems using Hybrid Power Flow Controller," in *Proc. Int. Conf. Power and Energy Systems (ICPS)*, pp. 1–6, Dec. 2011.

[12] G. Aggarwal, L. Mathew, and S. Chatterji, "MATLAB/Simulink based simulation of a Hybrid Power Flow Controller," in *Proc. Int. Conf. Advanced Computing & Communication Technologies (ACCT)*, pp. 523–531, Feb. 2014.

[13] Hydro One Incorporated, [Online]. Available: http://www.hydroone.com

[14] J. Bebic and P. Lehn, "Hybrid Power Flow Controller and method," U.S. Patent 6 963 187 B2, Nov. 8, 2005.

[15] PSCAD™/EMTDC™, Manitoba HVDC Research Centre, Program Website, [Online]. Available: https://hvdc.ca/pscad

[16] Simulink®-Simulation and Model-based Design, Program Website, [Online]. Available: http://www.mathworks.com/products/simulink/

[17] J. Bian, D. G. Ramey, R. J. Nelson, and A. Edris, "A study of equipment sizes and constraints for a Unified Power Flow Controller," *IEEE Trans. Power Del.*, vol. 12, no. 3, pp. 1385–1391, Jul. 1997.

[18] J. Y. Liu, Y. H. Song, and P. A. Mehta, "Strategies for handling UPFC constraints in steady-state power flow and voltage control," *IEEE Trans. Power Syst.*, vol. 15, no. 2, pp. 566–571, May 2000.

[19] X. Wei, J. H. Chow, B. Fardanesh, and A. Edris, "A common modelling framework of voltage-sourced converters for power flow, sensitivity, and dispatch analysis," *IEEE Trans. Power Syst.*, vol. 19, no. 2, pp. 934–941, May 2004.

[20] J. Z. Bebic, P. W. Lehn, and M. R. Iravani, "P-δ characteristics for the Unified Power Flow Controller-analysis inclusive of equipment ratings and line limits," *IEEE Trans. Power Delivery*, vol. 18, no. 3, pp. 1066–1072, Jul. 2003.

[21] S. Bhowmick, and B. Das, "An Indirect UPFC model to enhance reusability of Newton power-flow codes," *IEEE Trans. Power Del.*, vol. 23, no. 4, pp. 2079–2088, Oct. 2008.

[22] E. Uzunovic, C. A. Cañizares, and J. Reeve, "Fundamental frequency model of Unified Power Flow Controller," in *Proc. North American Power Symposium (NAPS)*, Cleveland, OH, pp. 294–299, Oct. 1998.

[23] C. A. Cañizares, "Power flow and transient stability models of FACTS controllers for voltage and angle stability studies," in *Proc. IEEE PES Winter Meeting*, Singapore, pp. 1447–1454, Jan. 2000.

[24] J. M. Maza-Ortega, A. Gómez-Expósito, M. Barragán-Villarejo, E. Romero-Ramos and A. Marano-Marcolini, "Voltage source converter-based topologies to further integrate renewable energy sources in distribution systems," *IET Renewable Power Generation*, vol. 6, no. 6, pp. 435–445, Nov. 2012.

[25] PSS®E 33, Program Application Guide, 2013.

[26] A. G. Expósito, A. J. Conejo, and C. Cañizares, *Electric Energy Systems, Analysis and Operation*. Boca Raton, FL., USA: CRC Press, 2009.

[27] J. Arrillaga and N. R. Watson, *Computer Modelling of Electrical Power Systems*. Delhi, India: Wiley, 2013.

[28] R. Battiti, M. Brunato, and F. Mascia, *Reactive Search and Intelligent Optimization*. New York: Springer, 2008.

[29] R. Fourer, D. Gay, and B. Kernighan, *AMPL: A Modeling Language for Mathematical Programming*. Pacific Grove, CA., USA: McGraw-Hill, 2003.

[30] General Algebraic Modeling System (GAMS), Program Website, [Online]. Available: http://www.gams.com/

[31] A. Yazdani and R. Iravani, *Voltage-sourced converters in power systems*. New York: John Wiley & Sons, 2010.

[32] M. Farrokhabadi, S. Koenig, C. A. Cañizares, K. Bhattacharya, and T. Leibfried, "Battery energy storage system models for microgrid stability analysis and dynamic simulation," *IEEE Trans. Power Syst.*, vol. 32, no. 5, pp. 1–13, Aug. 2017.

[33] F. Milano, "An open source power system analysis toolbox," *IEEE Trans. Power Syst.*, Vol. 20, No. 3, pp. 1199–1206, Aug. 2005.

[34] Federico Milano's Website, [Online]. Abailable: http://faraday1.ucd.ie/psat.html

[35] UWPFLOW, Continuation and Direct Methods to Locate Fold Bifurcations in AC/DC/FACTS Power Systems, Program Website, [Online]. Available: https://ece.uwaterloo.ca/ ccanizar/software/pflow.htm

[36] Artelys Knitro, Program Website, [Online]. Available: https://www.artelys.com/

[37] B. Tamimi, C. A. Cañizares, and S. Vaez-Zadeh, "Effect of reactive power limit modeling on maximum system loading and active and reactive power markets," *IEEE Trans. Power Syst.*, vol. 25, no. 2, pp. 1106–1116, Feb. 2010.

[38] Python, Program Website, [Online]. Available: https://www.python.org/

[39] "Hybrid Power Flow Controller, PSS/E power flow model documentation," Electranix, Winnipeg, Manitoba, Canada, May 2013.

[40] P. Kundur, *Power System Stability and Control*. New York: McGraw-Hill, 1994.

[41] Ontario Independent Electricity System Operator (IESO), [Online]. Available: http://www.ieso.ca

[42] M. Eslami, H. Shareef, A. Mohamed, and M. Khajehzadeh, "A survey on flexible ac transmission systems (FACTS)," *Przeglad Elektrotechniczny*, Issue 01a, pp. 1–11, Jan. 2012.

[43] "Flexible ac transmission systems benefits study," San Diego Gas and Electric, San Deigo, CA., USA, Oct. 1999.

[44] R. M. Mathur and R. K. Varma, *Thyristor-Based FACTS Controllers for Electrical Transmission Systems*. Piscataway, NJ: Wiley-IEEE Press, 2002.

[45] M. Borage, S. Tiwari, and S. Kotaiah, "Constant-current, constant-voltage half-bridge resonant power supply for capacitor charging," in *Proc. IEE Electric Power Applications*, vol. 153, no. 3, pp. 343–347, May 2006.

[46] T. Gönen, *Electric power distribution engineering*. Third Ed., Boca Raton, FL: CRC Press, 2014.

[47] K. Strunz, "Developing benchmark models for studying the integration of distributed energy resources," in *Proc. IEEE PES General Meeting*, Montreal, Quebec, Canada, pp. 1–2, 2006.

[48] B. Tamimi, C. A. Cañizares, and K. Bhattacharya, "System stability impact of large-scale and distributed solar photovoltaic generation: The case of Ontario, Canada," *IEEE Trans. Sustain. Energy*, vol. 4, no. 3, pp. 680–688, Jul. 2013.

[49] J. V. Milanovic and Y. Zhang, "Modeling of FACTS devices for voltage sag mitigation studies in large power systems," *IEEE Trans. Power Del.*, vol. 25, no. 4, pp. 3044–3052, Oct. 2010.

[50] *IEEE Guide for Voltage Sag Indices*, IEEE Standard 1564, 2014.

[51] J. C. Gomez and M. M. Morcos, "Voltage sag and recovery time in repetitive events," *IEEE Trans. Power Del.*, vol. 17, no. 4, pp. 1037–1043, Oct. 2002.

[52] "Solar eclipse readiness," California ISO, Public report, Aug. 2017 [Online]. Available: http://www.caiso.com

[53] B. Tamimi and C. A. Cañizares, "HPFC power flow modeling," Technical Report, Prepared for Hydro One Inc., 40 pages single-column, 2013.

[54] B. Tamimi and C. A. Cañizares, "Practical application of the Hybrid Power Flow Controller," in *Proc. IEEE PES General Meeting*, Boston, MA, USA, pp. 1–5, 2016.

[55] B. Tamimi, C. A. Cañizares, and C. Battistelli, "Hybrid Power Flow Controller steady-state modeling, control, and practical application," *IEEE Trans. Power Syst.*, vol. 32, no. 2, pp. 1483–1492, Mar. 2017.

[56] B. Tamimi and C. A. Cañizares, "Modeling and application of Hybrid Power Flow Controller in distribution systems," Submitted to *IEEE Trans. Power Del.*, 8 pages double-column, Oct. 2017.

APPENDICES

Appendix A

Two-area System Data

Tables A.1 to A.5 show the data for the 60 Hz test system depicted in Figure A.1. The bases for the system parameters are 100 MVA and 20kV/230kV.

Table A.1: Generators

Bus No.	P_G [p.u.]	V [p.u.]	Q_{Gmax} [p.u.]	Q_{Gmin} [p.u.]
1	7	1.03	5	-2
2	7	1.01	5	-2
3	Slack	1.03	–	–
4	7	1.01	5	-2

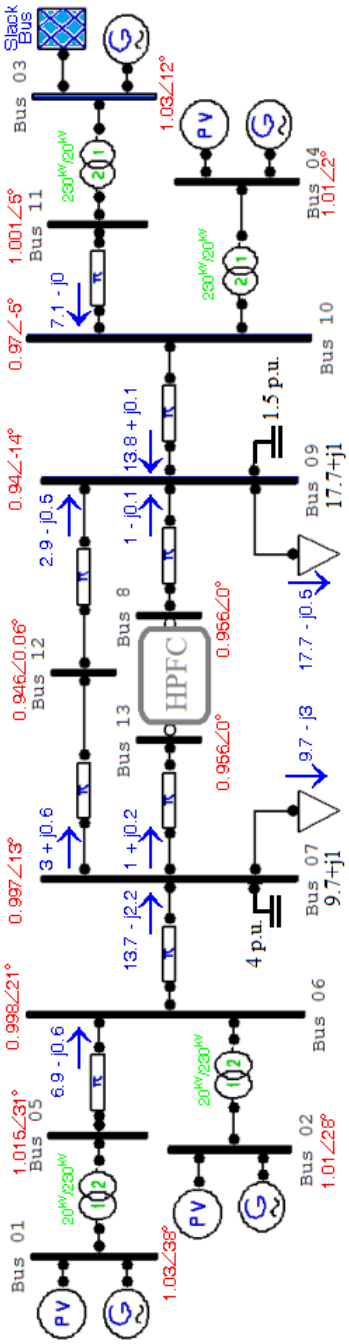

Figure A.1: Detailed single-line-diagram of the two-area test system.

Table A.2: Slack generator

Bus No.	V [p.u.]	δ [rad]
3	1.03	-0.1187

Table A.3: Loads

Bus No.	P_D [p.u.]	Q_D [p.u.]
7	9.67	-3
9	17.67	-0.5

Table A.4: Transmission lines and transformers

Bus_{Fr}	Bus_{To}	r [p.u.]	x [p.u.]	b [p.u.]
5	6	0.0025	0.025	0.04375
6	7	0.001	0.01	0.0175
7	12	0.00733	0.0733	0.1925
12	9	0.00733	0.0733	0.9625
8	9	0.022	0.22	0.1925
11	10	0.0025	0.025	0.04375
9	10	0.001	0.01	0.0175
7	13	0.022	0.22	0.09625
1	5	0	0.0167	0
2	6	0	0.0167	0
4	10	0	0.0167	0
3	11	0	0.0167	0

Table A.5: Generator cost $C\left(P_G\right) = a + bP_G + cP_G^2$

Bus No.	a [\$/h]	b [\$/MWh]	c [\$/MW^{2}h]	P_{Gmax} [MW]
1	800	20	0.002	2000
2	800	20	0.002	2000
3	1600	40	0.004	2000
4	1600	40	0.004	700

Appendix B

Potential HPFC Locations in Ontario

Four potential areas of the grid for further study to assess the performance of the HPFC as per Figure 3.14, based on PV-curves and related studies performed for different loading scenarios:

a. Ottawa's 115 kV circuits: These lines provide a looped connection from Hawthorne. Under normal system conditions, one of the circuits supplies Cyrville, the National Research Council and approximately half the load at Bilberry Creek. The other circuit supplies Naven, Wilhaven, Rockland, Cumberland and the remaining half of Bilberry Creek. Cyrville also has a supply from this 115 kV circuit, between Hawthorne and King Edward. Under outage conditions involving one of the circuits, the other one would supply the entire Bilberry Creek load. As the load at these stations grows, the thermal loading of the circuits may be exceeded, and the voltage at the stations at the end of the circuits will be difficult to regulate.

b. Bell River's 115 kV circuits: These lines supply Belle River and Kingsville from Lauzon. One of the circuits also extends from Belle River Junction through to Tilbury, where it supplies Tilbury and Tilbury West. As the load at these stations grows, the thermal loading of the circuits will be exceeded, especially following the loss of one of the circuits, and the voltage at the stations at the end of the circuits will be difficult to regulate.

c. Burlington's 115 kV circuits: These lines supply Enbridge Westover, Puslinch, Arlen, Hanlon and half of Cedar from Burlington. Under outage conditions involving circuits that supply the other half of Cedar, all of the load at Cedar is supplied from these

circuits. As the load at these stations grows, the thermal loading of the circuits will be exceeded, especially following the loss of one of the circuits, and the voltage at the stations at the end of the circuits, in particular at Cedar, will be difficult to regulate.

d. Trafalgar's 230 kV circuits: These lines are located between Burlington, Trafalgar and Richview. Under conditions of high generation output in the southwest part of the province (e.g. maximum gas, wind, and even imports from Michigan) and low generation east of Toronto, (e.g. Pickering shutdown, one or two Darlington units out of service, Lennox out of service, and/or exports to Quebec), high power transfers along this transmission corridor can be observed, so that the loading could exceed the continuous pre-contingency rating, and thus exceed the short-term emergency post-contingency rating, following the outage of a single circuit or a pair of circuits on one of the double-circuit lines.

Appendix C

Distribution System Data

The test system data based on the 12.7 kV, 60 Hz CIGRE test system is shown in Tables C.1–C.2 for the system depicted in Figure 5.5.

Table C.1: Line parameters for the distribution test system

Bus		R'_{ph}	X'_{ph}	B'_{ph}	R'_0	X'_0	B'_{ph}	l
From	To	[Ω/km]	[Ω/km]	[μS/km]	[Ω/km]	[Ω/km]	[μS/km]	[km]
1	2	0.282	0.703	3.83	0.351	1.8	1.57	1.2
2	3	0.282	0.703	3.83	0.351	1.8	1.57	1
3	4	0.282	0.703	3.83	0.351	1.8	1.57	0.61
4	5	0.282	0.703	3.83	0.351	1.8	1.57	0.56
5	6	0.282	0.703	3.83	0.351	1.8	1.57	1.54
6	7	0.282	0.703	3.83	0.351	1.8	1.57	0.24
7	8	0.282	0.703	3.83	0.351	1.8	1.57	1.67
8	9	0.282	0.703	3.83	0.351	1.8	1.57	0.32
9	10	0.282	0.703	3.83	0.351	1.8	1.57	0.77
10	11	0.282	0.703	3.83	0.351	1.8	1.57	0.33
11	4	0.282	0.703	3.83	0.351	1.8	1.57	0.49
3	8	0.282	0.703	3.83	0.351	1.8	1.57	1.3
12	13	0.282	0.703	3.83	0.351	1.8	1.57	4.89
13	14	0.282	0.703	3.83	0.351	1.8	1.57	2.99
14	8	0.282	0.703	3.83	0.351	1.8	1.57	2

Table C.2: Loads power for the distribution test system

Bus	P [kW]	Q [kVAR]
1	144	69.3
2	159	81.9
3	38.4	28.8
4	$Subnetwork_1$*	
5	39.5	53.26
6	28.5	9.36
7	57	18.73
8	$Subnetwork_2$**	
9	57	18.73
10	81	39.3
11	105	57.36
12	183	96
13	74.1	45.82
14	48	24

* $Subnetwork_1$ demand is 108 kW and 2052.3 kVAR.
** $Subnetwork_2$ demand is 1054 kW and 1026 kVAR.